Three-Dimensional Tracer Structure and Behavior as Simulated in Two Ozone Precursor Experiments

J. D. MAHLMAN, H. LEVY II AND W. J. MOXIM

Geophysical Fluid Dynamics Laboratory/NOAA, Princeton, NJ 08540

(Manuscript received 4 June 1979, in final form 29 October 1979)

ABSTRACT

The GFDL 11-level general circulation/tracer model is used for two experiments designed to prepare the way for a self-consistent model of atmospheric ozone. The first experiment invokes a very simple condition at the top model level, an instantaneous relaxation to a specified 10 mb average observed ozone value. The tracer is inert below the top level until it is removed in the lower troposphere. The second experiment introduces a simplified, but reasonably realistic ozone chemistry at the top level including Chapman, nitrogen and hydrogen loss processes. Below the top level, ozone is inert, and is removed in the lower troposphere by the same mechanism as in the first experiment.

These two experiments, in spite of their very different middle stratospheres, show remarkably similar behavior in the lower stratosphere. A comparison of model values and fluxes with available observations shows general qualitative agreement as well as some notable discrepancies.

In the second experiment, a detailed analysis of the processes affecting the 10 mb zonal-mean mixing ratio is presented. The results show that the mid-stratospheric ozone production and losses are strongly sensitive to circulation features, changing overhead sun angle and temperature. These various effects lead to some substantial interhemispheric and seasonal asymmetries in the ozone production.

An analysis is performed of the transport processes leading to the pronounced poleward-downward slope of tracer isopleths. The results demonstrate that adiabatic and diabatic effects in the eddies, as well as diabatic effects in the zonal mean, all contribute importantly to the creation of these sloping surfaces.

As an aid to tracer transport analysis, a Lagrangian "non-transport" theorem is derived for an integration following a fluid particle. Some Lagrangian drift-type calculations are performed in the model January mean flow. The results show a slow but substantial particle convergence just to the cyclonic shear side of the time-mean jet stream axis. This is a region where the traditional zonal-mean budget analysis shows a very large cancellation between eddy and meridional circulation flux convergence. Also, the analysis demonstrates indirectly the very important contributions of transient disturbances to the movement of heat and tracers irreversibly into the stratospheric polar vortex.

1. Introduction

In spite of the significantly increased attention ozone has received over the last decade or so, a fully quantitative understanding of its structure remains unavailable. This is because a successful model of ozone must treat properly the interactive radiative-chemical-dynamical system in the troposphere, stratosphere and possibly the mesosphere. Although such models are being attempted, their fully successful completion requires much further progress.

In the meantime, all attempts at quantitative ozone modeling incorporate substantial simplifications depending upon which aspects of the problem are chosen for emphasis. An excellent example of these simplifications may be found in the so-called one-dimensional (1-D) chemical models incorporating severely parameterized transport and space-time averaged chemistry. These models have been in-

valuable in sorting out some of the uncertainties and the irrelevancies contained in the complex chemical equations.

In a similar vein, models which emphasize 3-D atmospheric transport at the expense of exhaustive chemical detail are also extremely valuable. They provide a mechanism for assessing errors in modeling atmospheric motions and also provide a means for evaluating which types of motions are dominant in the problem. Examples of this approach are given in Hunt and Manabe (1968), Hunt (1969), Clark (1970), Mahlman (1973a), London and Park (1973, 1974), Cunnold *et al.* (1975), Mintz and Schlesinger (1976), Kao *et al.* (1976), Kida (1977a,b), Mahlman and Moxim (1978) and Schlesinger and Mintz (1979). Of the above models which emphasized ozone, only the quasi-geostrophic model of Cunnold *et al.* (1975) was integrated long enough to achieve a satisfactorily equilibrated state over the seasons. Thus,

only that model can be used for a meaningful comparison with the long-term results of this study.

The work presented in this paper incorporates the 3-D approach, and is the beginning of a series of increasingly complex experiments designed to investigate many aspects of the ozone problem. The basic tool employed is the GFDL 3-D tracer model as described in some detail in Mahlman and Moxim (1978, hereafter referred to as MM78). A description of the stratospheric behavior of the general circulation model (whose winds are used purely as input for the tracer model and are not affected by the tracer structure) is given in Manabe and Mahlman (1976, hereafter MM76). For a list of references to other publications on the performance of this GCM, see MM78.

A major goal of the experiments performed here is to evaluate various aspects of the physical mechanisms responsible for transport of ozone in the atmosphere. Topics emphasized in this paper involve comparison with observation, the interaction between chemistry and transport in the middle stratosphere, transport of ozone to the troposphere, mechanisms responsible for the poleward-downward slopes of constant ozone surfaces, and some differences in interpretation between Eulerian and Lagrangian views of tracer transport. In addition, the effect of the drastically different source prescriptions in the model middle stratosphere on the ozone structure in the lower stratosphere will be presented through comparison of the two experiments.

2. Design of the experiments

a. Stratified Tracer experiment

The motivation for this experiment was to evaluate the conjecture that most of the climatological features of the ozone distribution in the lower stratosphere are the result of the action of stratospheric motions on the high degree of vertical stratification of the ozone mixing ratio. This stratification initially occurs as a result of a strong photochemical production of ozone in the middle stratosphere and net destruction in the troposphere.

In this experiment, the effect of a rapid photochemical response in the middle stratosphere is very crudely simulated by specifying a constant mixing ratio (R) everywhere at the top model level $(\sigma = p/p_* = 0.01 \approx 31$ km ≈ 10 mb)[1]. At the model interface level below the top level, a vertical flux of tracer is calculated. If the model calculates a flux of tracer out of the top level, the source term is

specified to be such that it just balances the advective loss. At the top model level, the tracer may be visualized as damping back instantaneously to its simple photochemical equilibrium value after being disturbed by a vertical transport process.

In the other stratospheric model levels, the tracer is specified to have no sources or sinks. Thus, the experimental design crudely simulates a very rapid transition in the vertical between an advection-dominated region (lower stratosphere) and a photochemical equilibrium region (middle stratosphere).

The choice of the constant value to be specified at the top level is completely arbitrary. To facilitate comparison with the Simple Ozone experiment, a value of 7.5 parts per million by volume (ppmv) is specified. This is close to the global-average mixing ratio at the 10 mb level as simulated in the second experiment. Some results from the first year of this experiment are presented in Mahlman (1973a). In that paper the top level mixing ratio was set equal to 1.0, expressed in arbitrary units.

In this experiment, the final tracer structure is not dependent on the initial condition. However, the integration time required to approach equilibration is dependent on the initial state. The initial condition on 1 August for this Stratified Tracer experiment is specified according to the simple quadratic function

$$R(K) = 7.5 \frac{(12 - K)^2}{121} , \qquad (2.1)$$

where K is a level index ranging from 1 at the top level to 11 at the bottom level next to the ground. The pressures to which these values of K correspond are given by $p(K) = 1000\sigma(K)$. Thus, at the initial state, the data are interpolated to the σ surfaces in such manner that there are no horizontal gradients of tracer on isobaric surfaces. This type of initial condition was chosen to help clarify the processes which act to establish the well-known poleward-downward slopes of quasi-conservative tracers in the lower stratosphere.

b. Simple Ozone experiment

1) BASIC DESCRIPTION

In this experiment, rather than specifying the O_3 mixing ratio of the top level to be a constant, a realistic but simplified photochemistry is used. Its inclusion permits the O_3 mixing ratio in the top level of the model to vary with longitude, latitude and season due to changing insolation and temperature. The O_3 photochemical production and destruction equations are solved at 10 mb, but the resulting net destruction or production of O_3 is treated as a mean net rate for the top layer which extends from 0 to 27.6 mb.

The Simple Ozone experiment is an attempt to

---

[1] As described in MM76 and MM78, the model is expressed in sigma coordinates ($\sigma = p/p_*$, where p is pressure and p_* is surface pressure). The approximate pressures corresponding to the model sigma levels can be seen in Fig. 3.1.

study the effects of photochemistry in the top level (middle stratosphere) on O_3 transport. It is not meant to simulate a quantitatively accurate O_3 climatology or the response of O_3 to a perturbation in photochemistry. Therefore, a detailed and highly accurate chemical scheme is not appropriate nor, given the state of O_3 photochemistry when the experiment began in 1975, even possible. Ozone production and Chapman destruction are calculated directly, while a partially parameterized non-Chapman destruction is calculated using constant mixing ratios for H_2O and NO_y ($NO + NO_2 + HNO_3$). H_2O is set at a constant 3 ppmv. Because of limited data and the desire to minimize the number of adjustable parameters, a constant value for the NO_y mixing ratio is used at all latitudes. This value of NO_y (17.5 ppbv) is the one which, when using this chemistry, produces model equatorial 10 mb O_3 in agreement with observations. However, in a purely photochemical calculation, this value of NO_y gives O_3 values in excess of those observed at low latitudes. This excess is necessary to balance the net transport removal of ozone from the 10 mb tropics.

The ability of this chemical model to generate a realistic net photochemical source in the middle stratosphere and capture the appropriate time scales is partially insulated from the frequent changes in measurements of specific reaction rate coefficients, absorption cross sections and species concentrations. For example, when this model was constructed in 1975, NO_x was thought to dominate non-Chapman destruction, with some contribution from HO_x and very little from CLO_x (e.g., Wofsy, 1974). Currently, due to both new measurements of reaction rate coefficients and new reactions, NO_x, CLO_x and HO_x are all thought to be important and strongly coupled (e.g., Turco et al. 1978). While the model non-Chapman ozone destruction chemistry does not now agree in many details with the current view, the net effect of the required non-Chapman destruction at 10 mb was designed to be conserved by the explicit use of NO_y mixing ratio as an arbitrary parameter. This photochemical scheme is significantly more detailed than the one used by Cunnold et al. (1975) in their 3-D ozone model which specified NO_2, OH and HO_2 from earlier 1-D calculations. It is quite similar in many respects to the one used by London and Park (1974). One difference is their use of an estimated NO_x profile in comparison to this model's use of NO_y as an explicit parameter to guarantee the correct simulated O_3 mixing ratio at 10 mb in the tropics.

In order to isolate the effects of photochemistry in the middle stratosphere on O_3 transport processes in the lower stratosphere, no photochemistry is included in any of the other stratospheric levels. While this appeared to be justified by a comparison of transport and photochemical lifetimes, an *a posteriori* examination of the model results shows that photochemistry in the lower stratosphere is quite necessary for a proper simulation of both the O_3 profile and the total column.

2) CHEMICAL DESIGN

From the large number of reactions and reactants thought to be relevant to ozone photochemistry at 10 mb (e.g., Hampson and Garvin, 1975), the 17 chosen for this model are listed in Table 1. The photodissociation rate coefficients Ji at 10 mb are determined from the data sources given in Table 1 and solar flux data from Ackerman (1971) and Simon (1974). Daytime average Ji's are used so that destruction due to R9 is not overestimated (Kurzeja, 1975). However, the net daytime destruction or production is spread uniformly over the full 24 h period since the model does not have a diurnal cycle.

While Rayleigh and aerosol scattering of the downward flux are small enough to be neglected, for wavelengths $>310 \times 10^{-9}$ m the solar flux is multiplied by 1.3 as an approximate correction for backscatter by the earth's surface and lower atmosphere. Above 6 mb the total column of O_3 is assumed to be constant using values based on the data of Heath (1974) and our own analysis. Between 6 and 10 mb, ozone is assumed to have a mixing ratio equal to the value calculated at 10 mb for the previous time step.

Using the 17 reactions listed in Table 1, the photochemical production of R ($= R_{O_3} + R_O$) is given by

$$\text{SOURCE} = 2 \cdot J1 \cdot R_{O_2}. \qquad (2.2)$$

The photochemical destruction of R is given by

$$\text{SINKS} = [2 \cdot R_{O_3} \cdot R_O \cdot K4 + 2 \cdot R_O \cdot R_{NO_2} \cdot K9$$
$$+ R_{OH}(K14 \cdot R_{O_3} + K16 \cdot R_O)$$
$$+ R_{HO_2}(K15 \cdot R_{O_3} + K17 \cdot R_O)] \cdot n(m), \qquad (2.3)$$

where $n(m)$ is the atmospheric number density and reaction R12 is neglected as a loss reaction. These two equations are then used in the continuity equation for R at the top level of the tracer model [see MM78, Eq. (3.7) and Section 3, for details].

A series of steady-state approximations are now made at each time step to solve for the mixing ratios R_{O_3}, R_O, R_{NO_2}, R_{OH} and R_{HO_2} used in Eq. (2.3).

Assuming the ratio of R_{O_3} to R_O is in steady state gives

$$R_O/R_{O_3} = J3/[R_{O_2} \cdot K2 \cdot n(m)^2]. \qquad (2.4)$$

$R = R_{O_3} + R_O$ and Eq. (2.4) are used to solve for the Chapman destruction in Eq. (2.3).

Assuming R_{OH} plus R_{HO_2} is in steady state relative to R and the ratio R_{HO_2}/R_{OH} is in steady state relative to R_{OH} plus R_{HO_2}, the ratio R_{HO_2}/R_{OH} is then given by

TABLE 1. Stratospheric ozone photochemistry.

Chapman photochemistry

R1	$O_2 + h\nu \rightarrow 2O$	$J1 = 4.7 \times 10^{-11}$*	Ackerman (1971)
R2	$O + O_2 + m \rightarrow O_3 + m$	$K2 = 1.0 \times 10^{-34}e^{(500/T)}$††	Hampson and Garvin (1975)
R3	$O_3 + h\nu \rightarrow O + O_2$	$J3 = 7.6 \times 10^{-4}$*	Ackerman (1971)
R4	$O + O_3 \rightarrow 2O_2$	$K4 = 1.9 \times 10^{-11}e^{-(2300/T)}$†	Hampson and Garvin (1975)

Nitrogen photochemistry

Partitioning of NO_y

R5	$NO + O_3 \rightarrow NO_2 + O_2$	$K5 = 9.0 \times 10^{-13}e^{-(1200/T)}$†	Hampson and Garvin (1975)
R6	$NO_2 + h\nu \rightarrow NO + O$	$J6 = 1.3 \times 10^{-2}$*	Hampson and Garvin (1975)
R7	$OH + NO_2 + m \rightarrow HNO_3 + m$	$K7 = 2.3 \times 10^{-30}(300/T)^{2.5}$††	Anderson et al. (1974)
R8	$HNO_3 + h\nu \rightarrow OH + NO_2$	$J8 = 8.6 \times 10^{-6}$*	Johnston and Graham (1973)

Ozone destruction

R9	$NO_2 + O \rightarrow NO + O_2$	$K9 = 9.1 \times 10^{-12}$†	Hampson and Garvin (1975)

Water chemistry

Radical source

R10	$O_3 + h\nu \rightarrow O(^1D) + O_2$	$J10 = 2.2 \times 10^{-4}$*	Ackerman (1971), quantum yields from Levy (1974)
R11	$O(^1D) + m \rightarrow O(^3P) + m$	$K11 = 6 \times 10^{-11}$†	Hampson and Garvin (1975)
R12	$O(^1D) + H_2O \rightarrow 2OH$	$K12 = 3.5 \times 10^{-10}$†	Hampson and Garvin (1975)

Radical sink

R13	$OH + HO_2 \rightarrow H_2O + O_2$	$K13 = 2 \times 10^{-10}$†	Hochanadel et al. (1972)

Ozone destruction/radical partitioning

R14	$OH + O_3 \rightarrow HO_2 + O_2$	$K14 = 1.6 \times 10^{-12}e^{-(1000/T)}$†	Hampson and Garvin (1975)
R15	$HO_2 + O_3 \rightarrow OH + 2O_2$	$K15 = 2.0 \times 10^{-13}e^{-(1500/T)}$†	estimated
R16	$OH + O \rightarrow H + O_2$	$K16 = 5.0 \times 10^{-11}$†	Kaufman (1969)
R17	$HO_2 + O \rightarrow OH + O_2$	$K17 = 6.0 \times 10^{-11}$†	Kaufman (1969)

* Daytime average rate for summer and 0° latitude (s⁻¹).
† Units are cm^3 molecule⁻¹ s⁻¹.
†† Units are cm^6 molecule⁻² s⁻¹.

$$RATIO_{HO_x} \equiv R_{HO_2}/R_{OH}$$

$$= \frac{K16 \cdot R_0 + K14 \cdot R_{O_3}}{K17 \cdot R_0 + K15 \cdot R_{O_3}}. \quad (2.5)$$

It is further assumed, based on 1975 rate coefficient data, that

$$R_{NO} \cdot K18 \ll [K17 \cdot R_0 + K15 \cdot R_{O_3}], \quad (2.6)$$

where $K18$ is the rate coefficient for

$$HO_2 + NO \rightarrow OH + NO_2. \quad (R18)$$

The OH mixing ratio is then given by

$$R_{OH} = [J10 \cdot R_{O_3} \cdot R_{H_2O} \cdot K12/(RATIO_{HO_x}$$
$$\cdot K11 \cdot n(m) \cdot K13)]^{1/2}. \quad (2.7)$$

Both R_{OH} and R_{HO_2} are then substituted into the water destruction portion of Eq. (2.3).

For the NO_2 loss path in (2.3) it is assumed that the partitioning of R_{NO}, R_{NO_2} and R_{HNO_3} is in steady state relative to the transported variable, R_{O_3} plus R_O. This is an excellent approximation for NO and NO_2, which adjust on time scales of a few minutes, but just adequate for HNO_3, which has a relaxation time

scale of 1–3 days in the sunlit middle stratosphere. With these assumptions,

$$R_{NO_2} = \frac{17.5 \times 10^{-9} \cdot B}{1 + B(1 + A)}, \quad (2.8)$$

where $R_{NO_y} = 17.5 \times 10^{-9}$ gives the correct equatorial R_{O_3} at 10 mb,

$$A \equiv J6/[K5 \cdot R_{O_3} \cdot n(m)], \quad (2.9)$$

$$B \equiv J8/[K7 \cdot R_{OH} \cdot n(m)^2]. \quad (2.10)$$

By neglecting $R_{NO} \cdot K18$ in Eq. (2.5) and solving Eqs. (2.4), (2.5), (2.7) and (2.8) in that order, it is possible to solve the steady-state equations, consistent with the reactions in Table 1, for R_{O_3}, R_O, R_{OH}, R_{HO_2} and R_{NO_2} in one pass. While a more detailed solution involving coupled equations and additional species such as $CLONO_2$, N_2O_5 and CLO is possible, it was neither justified nor necessary for this experiment as designed in 1975.

While there have been many changes in reaction rate coefficients, photodissociation rates and constituent concentrations since 1975 (e.g., Hudson, 1977), only four would have a significant impact on the current model at this time. The much larger
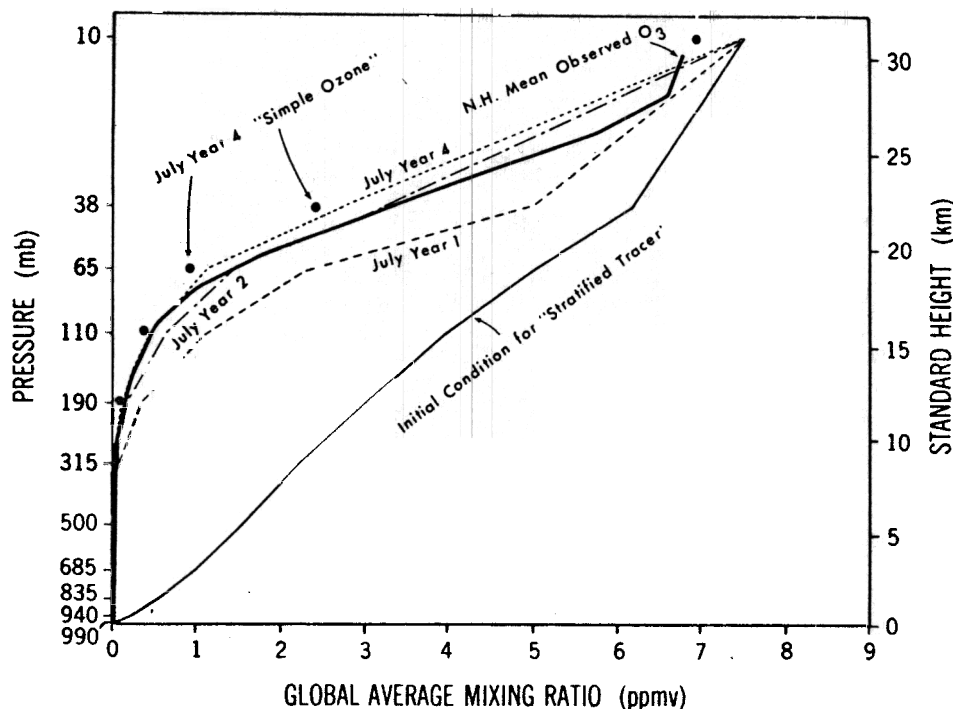
FIG. 3.1. Vertical distributions of the global-average mixing ratio from the Stratified Tracer experiment for the initial condition and July means of year 1, 2 and 4. Also shown are the Northern Hemisphere mean observed ozone [reanalyzed from Hering and Borden (1964, 1967)] and July year 4 from the Simple Ozone experiment (large dots).

value for $K18$ (Howard and Evenson, 1977) requires the inclusion of $R_{NO} \cdot K18$ in Eq. (2.5), which thus couples the nitrogen and water chemistry and increases R_{OH}. The measurements of CLO by Anderson et al. (1979) combined with the increased estimates of total chlorine in the stratosphere and decreased ratios of HCL/CLO found by recent photochemical models (e.g., Wofsy, 1978) point to an important role for CLO in ozone destruction and a strong coupling of the CL and N chemical cycles. The currently accepted estimate for $K13$ of 3.0×10^{-11} (Hudson, 1977) is much slower and leads to a significant increase in calculated R_{HO_x}. The most recent change, a large increase in the measured stratospheric value for $K15$ (Zahniser and Howard)[2], results in an increased role for HO_x destruction of O_3.

Incorporating these recent changes into the O_3 chemical model would increase its complexity and require an iterated solution of the steady-state equations. However, parameterization of total reactive nitrogen and chlorine would still be necessary. Therefore, if the photochemistry is to yield the correct 10 mb tropical O_3, the total non-Chapman destruction must remain the same, even using today's "improved" chemistry. In this way the

model's simulation of the non-Chapman destruction, by virtue of its NO_y parameterization, is partially buffered against uncertainties in the detailed mechanism.

c. Parameterization of tropospheric destruction.

One of the most surprising problem areas in atmospheric chemistry is the current inability to determine the basic facts of ozone production and destruction in the troposphere. In models such as the ones presented here, the best approaches for modeling tropospheric O_3 production and destruction are not at all obvious. However, the strong gradients of O_3 mixing ratio between stratosphere and troposphere lead to a net flux of O_3 downward across the tropopause. This net flux must be balanced by a net destruction in order to maintain the observed O_3 amount.

Because of the very large uncertainty in any current scheme for calculation of this net tropospheric destruction, the removal parameterization described in MM78 has been retained for this experiment. This scheme was originally designed to approximate the removal mechanisms applicable to particulate radioactive tracers. A dry removal is incorporated in the planetary boundary layer. In addition, tracer is removed in the free atmosphere proportional to the local precipitation rate and local tracer amount.
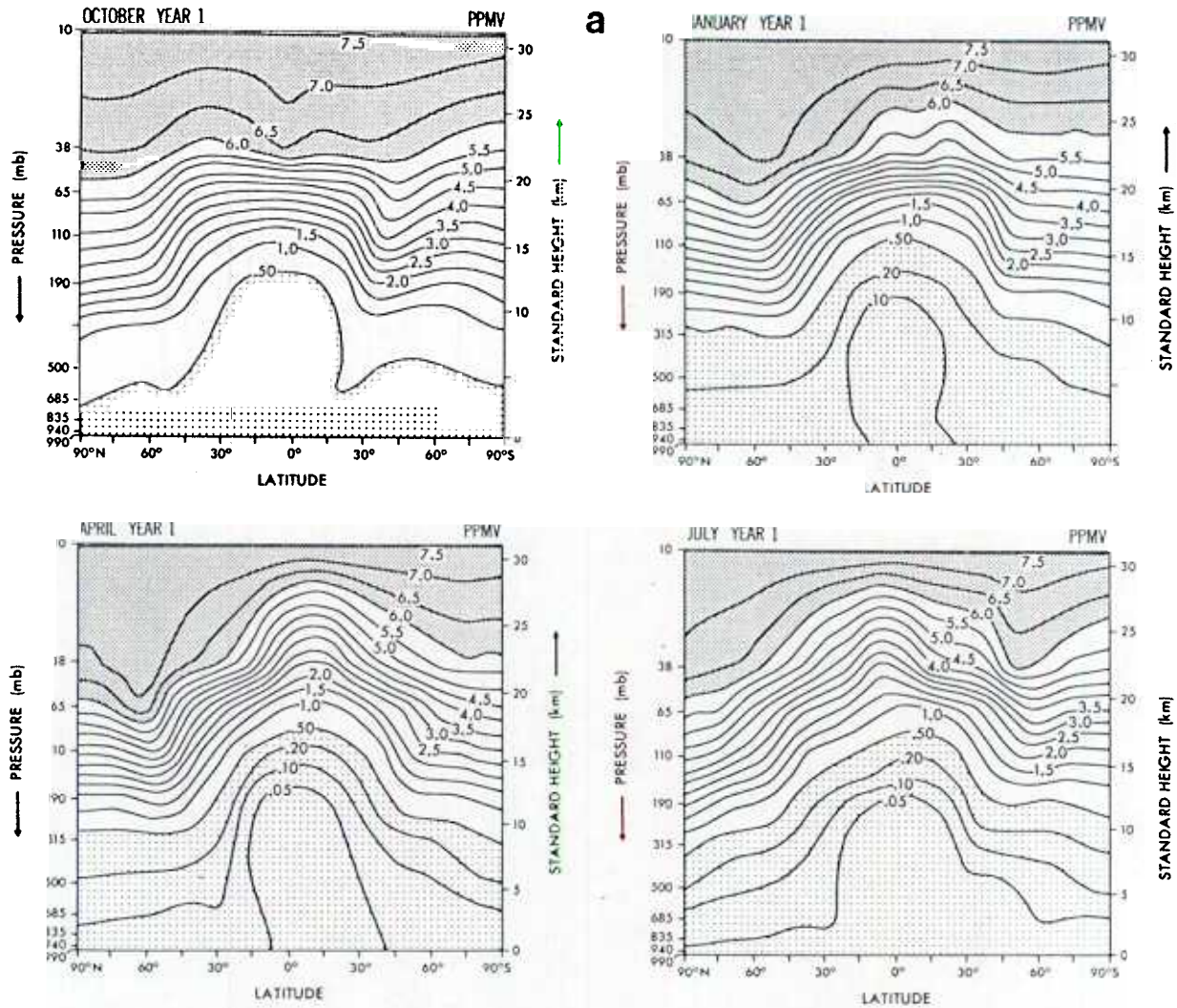
Zahniser and Howard (1979), private communication.

FIG. 3.2a. Zonal-mean mixing ratio (ppmv) for indicated months from the fourth year of the Stratified Tracer experiment Note logarithmic contour interval within lighter shading.

More specific details are given in MM78 as well as in Mahlman (1973a).

These removal processes, in many respects, are probably unlike those acting on atmospheric ozone. Nevertheless, the choice of this scheme was convenient because it allowed a more direct comparison with the tropospheric results of the midlatitude instantaneous source experiment described in MM78. In addition, the time scales of removal in this scheme are roughly consistent with those required to balance the tropospheric O_3 values against the stratospheric source of O_3 to the troposphere. Also, sensitivity tests with this model have shown that the stratospheric tracer structure is rather insensitive to the tropospheric removal efficiency over a considerable range of values. This is because, for a wide range of reasonable removal efficiencies, tropospheric air returning to the stratosphere tends

to be virtually depleted. However, in attempts to model *tropospheric* ozone amounts properly, a more correct formulation would become a very important consideration.

There appears to be no direct case that can be made for the precipitation related removal used in this scheme. In practice, such a scheme may have some crude semblance to reality because precipitating regions tend to occur in places where the intensity of vertical small-scale mixing is considerably greater than the average. Inasmuch as this early version of the model does not include explicit subgrid-scale vertical mixing, the scheme as presently constituted appears to compensate somewhat for this deficiency. In future ozone experiments, more realistic aspects of tropospheric chemistry will be included, along with a parameterization of the vertical mixing on subgrid scales.
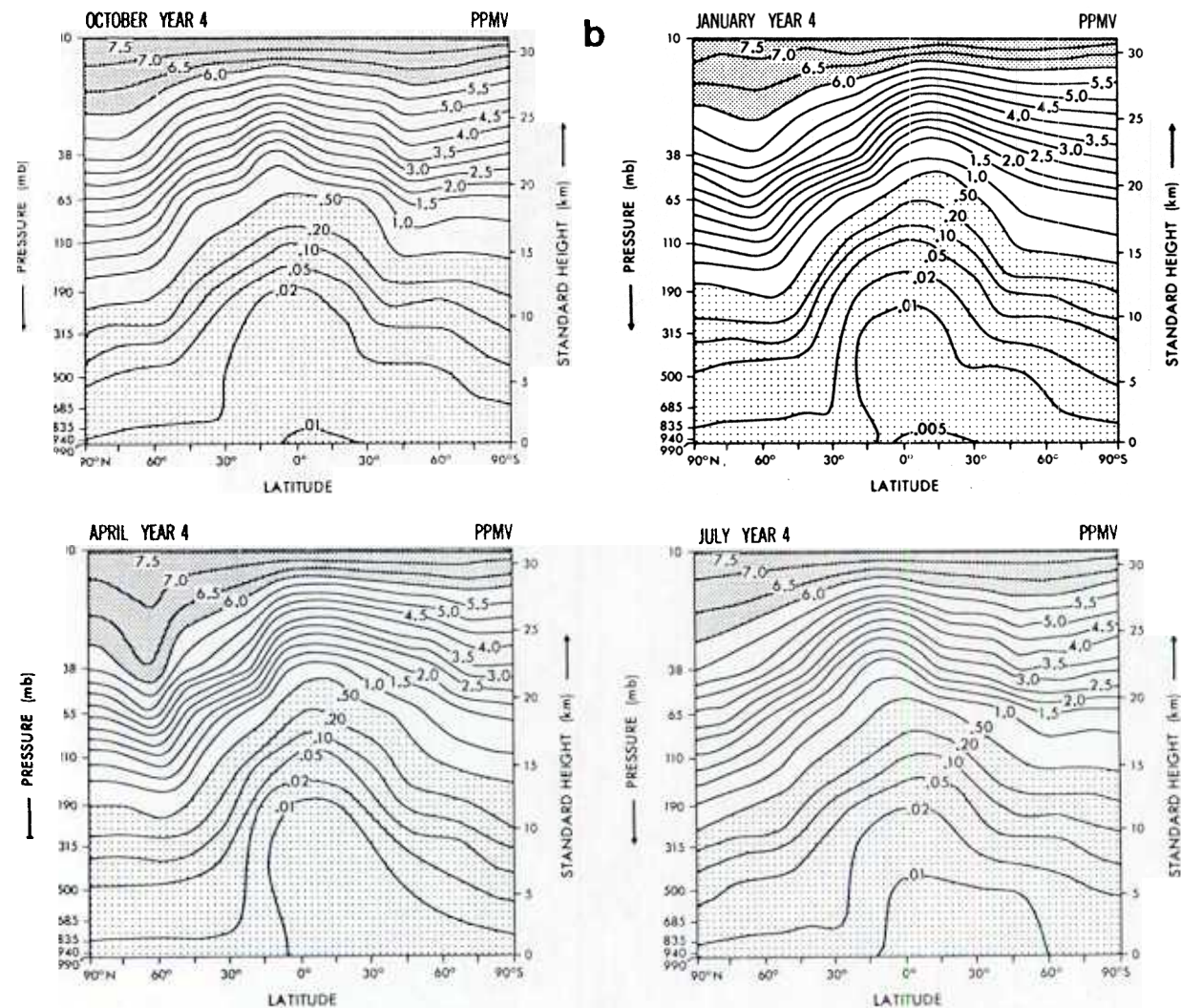
FIG. 3.2b. Zonal-mean mixing ratio (ppmv) for indicated months from the fourth year of the Stratified Tracer experiment

3. Basic results of the two experiments

a. Stratified Tracer large-scale structure

After the model starting time of 1 August, the adjustment of the tracer to the initial condition given in Eq. (2.1) is very rapid. Within about three days, the magnitude of horizontal tracer advection is the same as that of vertical advection, even though there are no horizontal tracer gradients initially. The impact of this rapid adjustment on the establishment of poleward tracer gradients is discussed in Section 5d.

The global average one-dimensional structure of the initial tracer distribution and the long-term response of the tracer in this experiment are given in Fig. 3.1. The profiles are for July at years 1, 2 and 4. The year 4 profile shows a reasonably close correspondence to the Northern Hemisphere mean O_3 given on the same figure. An identifiable differ-

ence is that the simulated tracer is less than the observed O_3 at 65 and 38 mb. A look at more detailed structure will later reveal, however, that some of this reasonably close agreement with observed O_3 is partly fortuitous.

Figs. 3.2a and 3.2b give the zonal-mean mixing ratio $(\bar{R}^\lambda)$ averaged over the months of October, January, April and July for the first and the fourth years of the experiment, respectively. In Fig. 3.2a, the October chart shows an evolution of considerable meridional structure by the third month of the experiment. Significant poleward increases of tracer are readily visible in the lower stratosphere. A pronounced downward protrusion of tracer is quite evident in the midlatitudes of the Southern Hemisphere, suggestive of efficient downward transport there in the late winter season. Efficient depletion of the tropical lower troposphere is quite evident. Specific mechanisms leading to the various zonal-
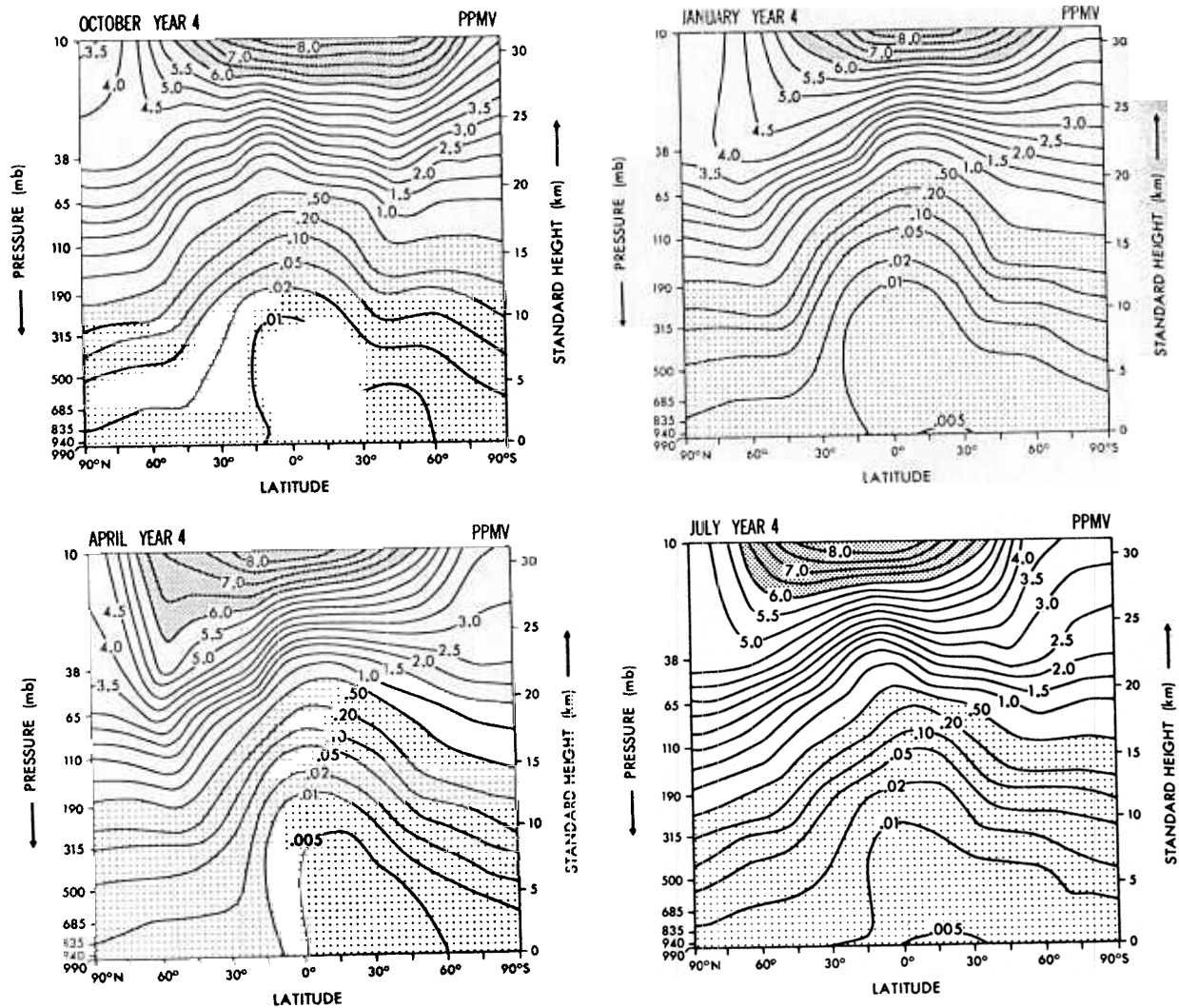
FIG. 3.3. Zonal-mean mixing ratio (ppmv) for indicated months from the fourth year of the Simple Ozone experiment.

mean features obtained here are discussed in Section 4a.

For January year 1, Fig. 3.2a shows a strong downward bulge of tracer near 60°N. Depletion of tracer in the troposphere continues in spite of significant downward transport near 50° in both hemispheres (see Mahlman, 1973a, Fig. 18). By April of year 1, the larger values in the Northern Hemisphere winter stratosphere are particularly evident. The equatorial maximum near 38 mb has now completely disappeared and has been replaced by relatively small values. In July of year 1, larger values in Southern Hemisphere winter are now quite evident, but the impact is not nearly as pronounced as in Northern Hemisphere January. Note that a significant amount of the high tracer values in Northern Hemisphere late winter remains into the summer period. Depletion of the troposphere is continuing, but now at a much slower rate than earlier in the experiment.

For October year 4, Fig. 3.2b shows a structure qualitatively similar to October year 1, but with some very important differences. The troposphere has now been depleted to very small values. Note that the entire troposphere is now contained within the last linear contour (0.5). The downward bulge in the Southern Hemisphere is much less pronounced than in October year 1. Also note that the downward bulge in the equatorial middle stratosphere has been replaced by relatively small values.

In January year 4, the average meridional gradients in the lower stratosphere are larger than in year 1. However, the slope of the lines is less steep locally during year 4 near 45°S. The Northern Hemisphere downward bulge is at a slightly higher latitude than during year 1, but the overall structure in that region is quite similar. In April year 4, the Northern Hemisphere structure is quite similar to that of year 1, but in the Southern Hemisphere the poleward-downward slopes of $\bar{R}^{\lambda}$ lines are diminished

considerably relative to year 1. For the Southern Hemisphere, the July year 4 chart shows a significant difference from the July year 1 structure in that the downward protrusion in midlatitudes is now far less apparent.

Overall, Fig. 3.2b shows that the Northern Hemisphere contains significantly more tracer than does the Southern Hemisphere. This is so in spite of the symmetry of the upper boundary condition and the use of a tropospheric sink parameterization whose only interhemispheric asymmetries are in the model precipitation [for the model's precipitation climatology, see Manabe and Holloway (1975)]. The major difference lies in the simulated Southern Hemisphere producing a considerably less efficient tracer transfer between the lower and middle stratosphere than does the Northern Hemisphere. Discussion of the reasons for these various model features is given in Section 4a.

b. Simple Ozone large-scale structure

This calculation was begun by imposing the 1 March year 2 field of the stratified tracer experiment. Thereafter, the two experiments were run in parallel.

The zonal-mean structure for year 4 of the Simple Ozone experiment is given in Fig. 3.3. In each of the four months shown, the effect of adding ozone chemistry in the middle stratosphere is quite evident, with highest values in the tropics and lower values elsewhere.

In the troposphere and lower stratosphere, the tracer structure is remarkably similar to that given in Fig. 3.2b for the Stratified Tracer experiment. This high degree of similarity and its implications will be discussed in further detail below.

The October year 4 field in Fig. 3.3 shows larger 10 mb $\bar{R}^{\lambda}$ values in the Southern Hemisphere, with relatively weaker meridional gradients than in the Northern Hemisphere. The lowered $\bar{R}^{\lambda}$ values in high latitudes at 10 mb can also be seen at 38 mb, but to a considerably lesser degree.

In January year 4, Fig. 3.3 shows that the 10 mb maximum in $\bar{R}^{\lambda}$ is centered nearer the equator than in October, but remains just in the Southern Hemisphere. At this time a strong asymmetry between the hemispheres is apparent. Between 38 and 10 mb in the Northern Hemisphere high latitudes, the vertical tracer gradient is very small, while in the Southern Hemisphere it is quite large.

By April the maximum in $\bar{R}^{\lambda}$ appears in the Northern Hemisphere. The remainder of the field appears quite similar to that of January in the same figure. The July year 4 $\bar{R}^{\lambda}$ distribution shows largest 10 mb values in the Northern Hemisphere. At 38 mb, the hemispheres are much more evenly balanced in July than in other seasons.

TABLE 2. Calculated correlation coefficients between the $\bar{R}^{\lambda}$ (Stratified tracer) and $\bar{R}^{\lambda}$ (Simple Ozone) values at each model analysis level for indicated months.

Pressure (mb)	October	January	April	July
38	0.942	0.992	0.952	0.955
65	0.996	0.996	0.997	0.992
110	0.996	0.994	0.999	0.996
190	0.985	0.984	0.989	0.997
315	0.960	0.985	0.956	0.996
500	0.996	0.990	0.989	0.991
685	0.932	0.971	0.990	0.980
835	0.986	0.993	0.997	0.987
940	0.969	0.987	0.993	0.977
990	0.956	0.963	0.975	0.978

As mentioned above, the $\bar{R}^{\lambda}$ structure below the middle stratosphere is very similar in the two experiments. To provide a measure of this, correlation coefficients were calculated at each analysis level comparing the calculated $\bar{R}^{\lambda}$ values in each experiment. The results are given in Table 2.

From these results, it is clear that the meridional structure of the troposphere and lower stratosphere in these experiments is almost completely insensitive to substantial changes in the manner in which the "chemistry" in the middle stratosphere is handled. These results suggest that it is the average stratification established between the middle stratosphere and the lower stratosphere that ultimately determines the horizontal tracer structure between. This is apparently because the time required for air to move from the middle stratosphere to the lower stratosphere is long compared to that required for horizontal tracer transfer within a hemisphere. Thus, a typical air parcel in the lower stratosphere will not have survived intact from a source region in the middle stratosphere. Its local mixing ratio would tend to reflect, to a first approximation, the average vertical tracer gradient between the lower and middle stratosphere, and the influence of the local meteorological conditions. A similar behavior was noted in MM78, in reference to the high correlations between their instantaneous source tracer and the local potential vorticity.

Although the above results show high correlations in the meridional structure between the two experiments at year 4, Fig. 3.1 and a closer inspection of Fig. 3.3 reveal that the average mixing ratios below the middle stratosphere are somewhat smaller in the Simple Ozone experiment (~15% at the end of the fourth year). Thus, even though the average mixing ratios at 10 mb are nearly the same and the sink parameterizations are identical, less tracer is transported out of the middle stratosphere in the Simple Ozone experiment.

This represents a deviation from idealized 1-D behavior, where the average flux is proportional to
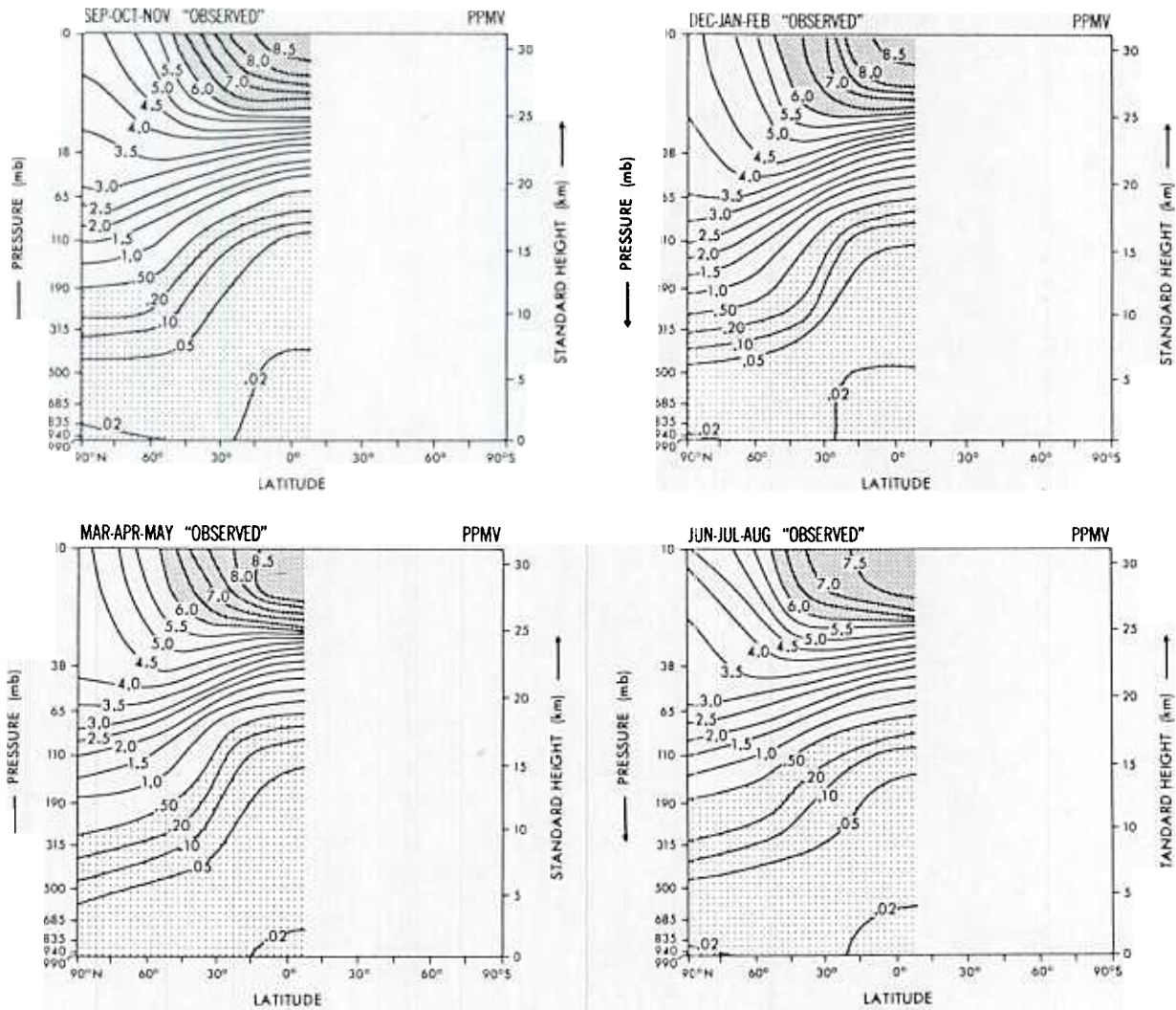
FIG. 4.1. Observed zonal-mean ozone mixing ratio (ppmv) for indicated seasons. Obtained by reanalysis of ozonesonde data from Hering and Borden (1964, 1967).

the average gradient. An analysis of the two experiments reveals that the difference arises because much of the downward transfer out of the "fast chemistry" region occurs in midlatitudes in association with planetary wave activity. It is the more realistic smaller 10 mb mixing ratios present in the Simple Ozone experiment (compared to the Stratified Tracer experiment) that lead to the smaller net downward flux calculated in the Simple Ozone experiment.

4. Comparison with observed ozone behavior

a. Seasonal evolution of zonal-mean ozone

Because ozone is by far the best documented stratospheric trace constituent, comparison of model results with available observations can provide especially meaningful tests. Unfortunately, the climatology of ozone is not known nearly as well

as it should be, particularly in the Southern Hemisphere. For example, the ozonesonde provides the only meaningful detailed measurements of ozone from the ground to the middle stratosphere. To date, however, the accuracy and the spatial-temporal density of the ozonesonde data have not been sufficient to provide unambiguous information on a number of aspects of ozone climatology. The best data coverage so far appears to be from the unfortunately short-lived North American Ozonesonde Network (Hering and Borden, 1964, 1967).

Presented in Fig. 4.1 are values of inferred zonal-time mean "observed" O_3 mixing ratio derived from that network. Zonal means of O_3 are estimated by the following procedure: The time averages for each network station are plotted at their appropriate geographical location every 2 km in height from 2 to 30 km. Isopleths of time-mean mixing ratio are then

subjectively analyzed over the North American area taking into account horizontal and vertical consistency, poor or insufficient data and stratospheric climatology. The O_3 structure in this region is then utilized to estimate the zonal-time mean at 10° latitude intervals.

Comparison of this "observed" O_3 structure in Fig. 4.1 to that of the Simple Ozone experiment given in Fig. 3.3 shows a number of interesting features. In general, the calculated values agree qualitatively with the observed. Large amounts are present in the equatorial middle stratosphere with decreasing values poleward. In the lower stratosphere, the poleward-downward slopes of the $\bar{R}^\lambda$ isopleths are similar. Sharply lower values are present in the troposphere in both computed and observed fields.

There are also model features which show disagreement between Figs. 4.1 and 3.3. In all seasons the poleward-downward slope of $\bar{R}^\lambda$ is somewhat too large. The model downward "bulge" of $\bar{R}^\lambda$ in higher northern latitudes is more pronounced, while values in the tropical lower stratosphere are somewhat too small. In the troposphere, O_3 values are generally too small, particularly in the tropics. However, recent measurements indicate much smaller lower troposphere O_3 values in the tropics than those shown in Fig. 4.1.[3]

Although it cannot be stated with certainty, the major discrepancies in the stratosphere appear to be related to the omission of ozone chemistry below the top model level. Inclusion of chemical effects at the lower levels would have the net effect of adding O_3 in the tropics and destroying it in high latitudes. In the troposphere, the discrepancies could be due either to the choice of removal mechanism, or to the omission of possible tropospheric ozone production mechanisms (e.g., Crutzen, 1973; Chameides and Walker, 1973).

For the seasonal evaluation, comparison of Figs. 4.1 and 3.3 shows some additional discrepancies. In October the polar values appear to be somewhat low at 10 mb and somewhat high at 38 mb. This has the effect of reversing $\partial \bar{R}^\lambda/\partial z$ relative to the observed in this region. The cause for this discrepancy is not presently clear. It could be either chemical or dynamical in origin. A further complication is that this region is one in which the observations are quite uncertain.

In January and April the same comparison shows a downward "bulge" near 60°N which is stronger than the observed. Near the highest latitudes, however, the simulated O_3 values are too small. This is probably in part related to the inability of the model to simulate the midwinter sudden stratospheric warming phenomenon (MM76). Also, the model's too cold
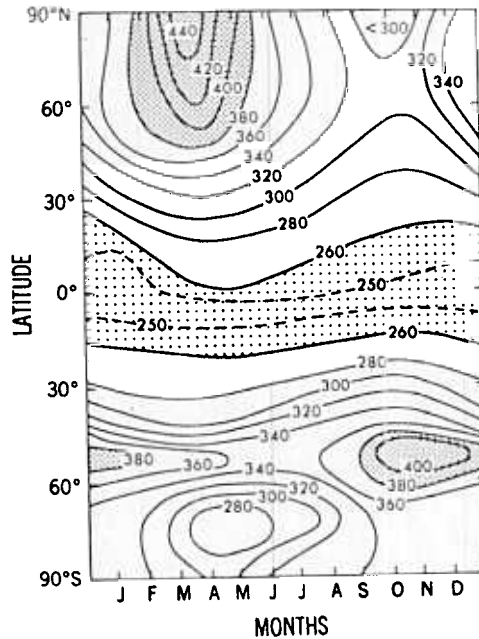

FIG. 4.2. Observed zonal-mean total ozone (10^{-3} atm-cm) for 12 months of the year. Redrawn from Dütsch (1969).

polar vortex leads to a larger poleward-upward slope of $\bar{\theta}^\lambda$ (potential temperature) surfaces than observed. This cold region can act to inhibit somewhat the simulated flux of tracer downward into the polar vortex, as will be shown in Section 5d. In July the model shows too much O_3 remaining in the high latitude lower stratosphere. This is probably a dynamical problem in that the lack of simulated midwinter sudden warmings leads to a late reversal to easterlies in the middle stratosphere (MM76). This delays the strong poleward-downward transport of O_3 to highest latitudes, thus higher values remain into the summer season. In addition, inclusion of chemical processes in the lower stratosphere would act to reduce this discrepancy.

b. Seasonal evolution of total ozone

It is of additional interest to compare the simulated total ozone against observations, particularly since a reasonable amount of Southern Hemisphere data are available. Fig. 4.2 shows the observed monthly zonal-mean total ozone as redrawn from Dütsch (1969). Although Dütsch cautions that errors are to be expected in the Southern Hemisphere, the data nevertheless reveal a number of important features. Most notable are the equatorial minimum and the considerably larger values in higher latitudes. In both hemispheres, pronounced seasonal effects are apparent. In addition, Fig. 4.2 shows pronounced interhemispheric asymmetries. The Northern Hemisphere shows an early spring maximum in high latitudes and a significant minimum in fall. The Southern

---
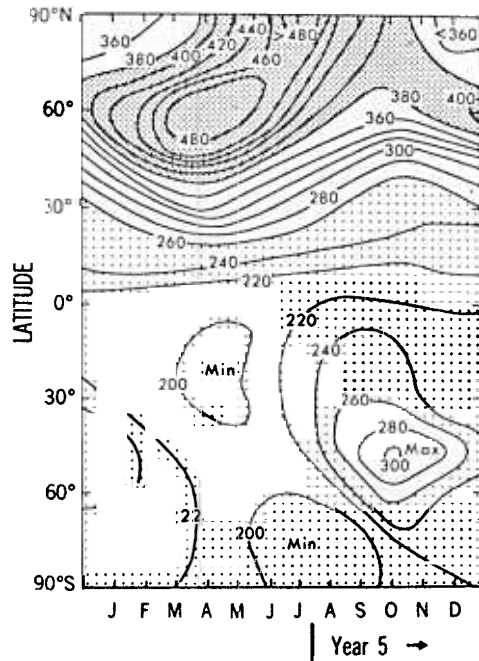
[3] D. D. Davis (1979), private communication.

FIG. 4.3. Simulated zonal-mean total ozone (10^{-3} atm-cm) for 12 months of the year as simulated in the Simple Ozone experiment.

Hemisphere exhibits a late spring maximum in midlatitudes with a rather pronounced late fall minimum in higher latitudes.

The corresponding structure from the Simple Ozone experiment is presented in Fig. 4.3. The Northern Hemisphere shows a pronounced early spring maximum near 60°N, which is somewhat larger than observation. The corresponding observed values show the maximum near or at the pole. It is not clear whether this discrepancy is due to the lack of a midwinter sudden warming in the model (MM76), a model deficiency in simulating mid-latitude transient disturbances (Hayashi and Golder, 1977), or to possible significant errors in the winter high-latitude total ozone observations. [See discussion by Dütsch (1969) on this possibility.] The model results show the effect of a pronounced poleward flux of O_3 in late spring associated with the simulated transition to summertime easterlies. The simulated fall minimum is slightly delayed compared to observation. In general, the model Northern Hemisphere contains more O_3 than observed. It is interesting that the quasi-geostrophic model simulation of Cunnold et al. (1975) shows closer agreement with the Dütsch (1969) Northern Hemispheric data than does this experiment.

In contrast to the Northern Hemisphere results, the model tropics and Southern Hemisphere show serious underpredictions of the total O_3. The Southern Hemisphere deficiency appears to be related to the GCM's tendency to overpredict the differences in stratospheric dynamical activity between the hemi-

spheres (MM76). In particular, the underprediction of Southern Hemisphere midwinter transient planetary wave activity appears to result in a deficient downward transport out of the mid-stratospheric "fast chemistry" region. One successful feature of the model is its prediction of the Southern Hemisphere spring maximum in midlatitudes, rather than higher latitudes as in the Northern Hemisphere. However, the amplitude of the seasonal variation appears to be somewhat overpredicted. In sharp contrast, the Southern Hemisphere high-latitude fall minimum is not present at all. The minimum shows up instead in late winter in the simulation. It is interesting to point out, however, that the satellite total ozone data presented by Prabhakara et al. (1976) show a late winter minimum and an early summer maximum in high southern latitudes, in qualitative agreement with this simulation.

Fig. 4.4 shows the spatial distribution of total O_3 for the months of July and December 1970 as determined by Prabhakara et al. (1976). Although these data contain systematic errors, many of the relative gradients are probably meaningful. In Fig. 4.5 are shown the equivalent quantities from the Simple Ozone experiment. For July the simulation shows only qualitative agreement with "observation" as shown in Fig. 4.4. The general meridional gradients are reasonably similar, but the longitudinal positions of various features appear to differ from observation in most important respects. It is interesting to note, however, that the Northern Hemisphere observed data of London (1963) for summer appears to differ as much from the July charts of Figs. 4.4 and 4.5 as the two figures differ from each other.

The corresponding comparison for December in Figs. 4.4 and 4.5 shows a considerable improvement for the Simple Ozone experiment in the Northern Hemisphere, while the Southern Hemisphere simulation appears as bad as July. The maximum off the east coast of Asia which extends into Alaska is quite well simulated. The minimum in the North Atlantic Ocean appears to be qualitatively correct. The equatorial minimum is too intense and may be displaced too far southward. The strong total ozone gradients in the Japan and Canadian east coast regions are associated with the tropospheric jet streams in these regions. This relationship between jet streams and total ozone gradients was pointed out by Lovill (1974), and is consistent with the jet stream and associated transverse circulation structure for this GCM as pointed out in Fig. 10.4 of MM76. See also Section 5e in this paper.

The Southern Hemisphere simulation is also deficient because the winter midlatitude peak has lasted into the summer season, while the observations show values increasing poleward to at least 60°S. The model seems to be too weak in its transport of O_3 to higher latitudes during the Southern Hemisphere spring transition.
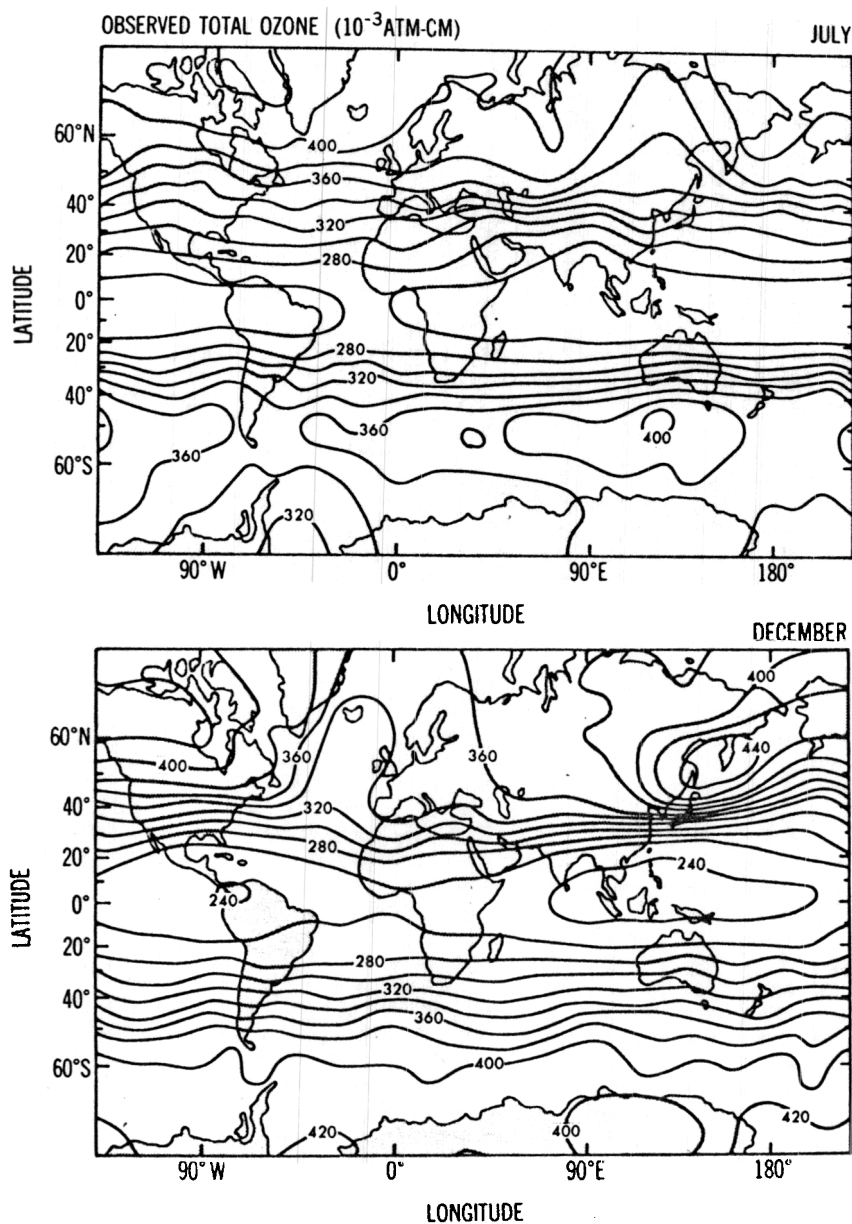
OBSERVED TOTAL OZONE (10⁻³ATM-CM)   JULY

DECEMBER

FIG. 4.4. Observed monthly mean satellite total ozone (10^{-3} atm-cm) for July 1970 and December 1970. Redrawn from Prabhakara et al. (1976).

c. Flux of ozone into the troposphere

Another interesting aspect of these experiments is an evaluation of the flux of O_3 from the stratosphere into the troposphere. As noted in Section 2c, the sources and sinks of ozone in the troposphere are highly uncertain. An improved understanding of the transport contribution can allow increased attention to the remaining large uncertainties in tropospheric ozone production and destruction.

The flux rates of O_3 into the upper troposphere as calculated over the last year of the Simple Ozone experiment are presented in Table 3. This table indicates that the average model global flux of 5.1

$\times 10^{14}$ molecules m^{-2} s^{-1} is strongly dominated by the Northern Hemisphere contribution of 6.6×10^{14}. The eddy flux contribution overwhelms the flux by

TABLE 3. Calculated annual mean vertical flux of ozone across the upper troposphere (actually the 240.6 mb surface) in the Simple Ozone experiment. Units: molecules m^{-2} s^{-1}.

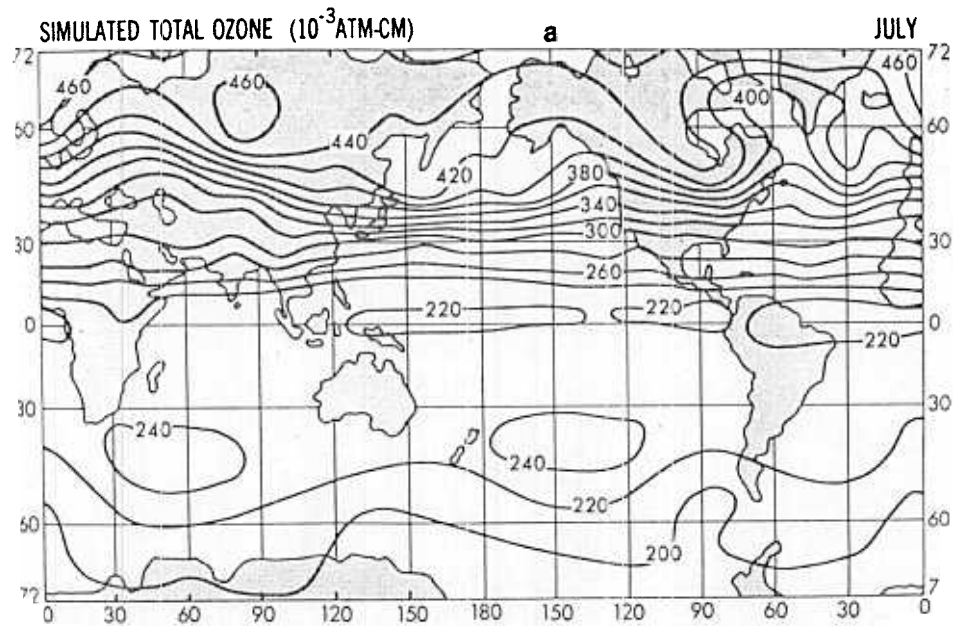| Region	Total flux	Meridional circulation flux	Eddy flux
Global	3.7×10^{14}	-0.1×10^{14}	3.8×10^{14}
Northern Hemisphere	4.8×10^{14}	-0.7×10^{14}	5.4×10^{14}
Southern Hemisphere	2.6×10^{14}	$+0.4 \times 10^{14}$	2.2×10^{14}

FIG. 4.5a. Simulated monthly mean total ozone (10^{-3} atm cm) for July year 4 from the Simple Ozone experiment.

the meridional circulation. The values given in Table 3 are similar to the observational estimates of mean Northern Hemisphere flux of 6.3×10^{14} molecules m^{-2} s^{-1} given by Reiter (1971) and 8×10^{14} from Danielson and Mohnen (1977). A global value of 6.6×10^{14} was obtained by Cunnold et al. (1975) in their simplified 3-D model ozone experiment.

Alternative estimates have been provided by analysis of the O_3 destruction rate in the surface boundary layer. For example, Aldaz (1969) estimates 10.1×10^{14}, while Fabian and Junge (1970) include a range of 3.5 to 5.9×10^{14} molecules m^{-2} s^{-1}. However, because of the possibility of significant ozone chemistry in the troposphere, boundary layer O_3 destruction is not a clear indicator of the cross-tropopause flux.

In view of the deficiencies of the Southern Hemisphere ozone simulation shown in Section 4, it is
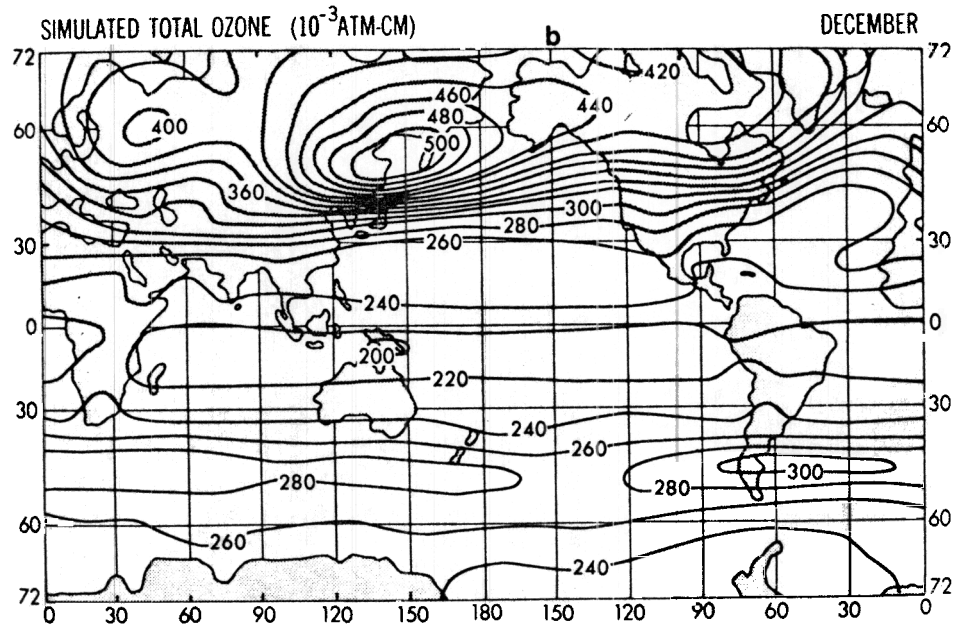

FIG. 4.5b. Simulated monthly mean total ozone (10^{-3} atm cm) for December year 4 from the Simple Ozone experiment.

probable that the Southern Hemisphere fluxes listed in Table 3 are too small. Some evidence consistent with this interpretation is presented by Fishman and Crutzen (1978), who suggest considerably larger Southern Hemisphere fluxes than obtained here.

5. Tracer transport mechanisms

a. 10 mb zonal-mean balances

Although the Simple Ozone experiment incorporates some simplifications in the ozone chemistry, and the 10 mb level of the model is subject to vertical resolution limitations, this level remains of considerable interest. In this calculation and in the real atmosphere, 10 mb is a level at which chemical processes and transport processes are characterized by similar time scales. Because it is the presence of transport processes which allows a net production of O_3 in the middle stratosphere, the response of the chemistry to these processes over the seasons of the year is required to gain a quantitative understanding of stratospheric ozone.

Fig. 5.1 shows the evolution of the zonal-mean ozone mixing ratio at 48°N over the year of the Simple Ozone experiment. The calculation shows an annual cycle with a minimum in December and a maximum in July. This latitude was chosen for emphasis because of the excellent O_3 climatology for Switzerland computed from a 6-year series of ozonesonde ascents compiled by Dütsch (1974). The monthly means from this data set given in Fig. 5.1 show reasonable agreement with the Simple Ozone experiment except during the months of December and January. There, the Dütsch data shows a secondary maximum. If this secondary maximum is real, its cause is not presently clear. Also given in Fig. 5.1 is the predicted evolution of $\bar{R}^\lambda$ (48°N) if the chemistry used in the Simple Ozone experiment were the only process acting. This chemistry-only calculation shows a similar annual cycle to the Simple Ozone
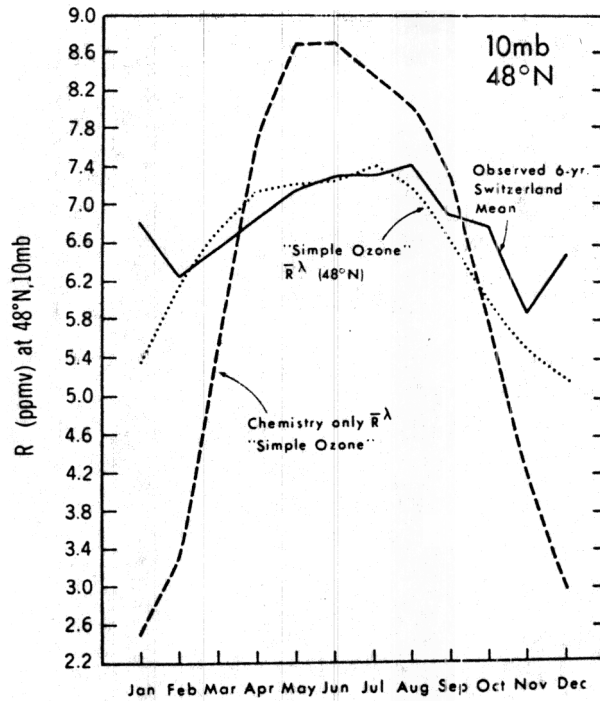

FIG. 5.1. Annual evolution of the zonal-mean ozone mixing ratio at 10 mb, 48°N. The dashed line shows the zonal-mean ($\bar{R}^\lambda$) obtained from the Simple Ozone chemistry only. Dotted line is $\bar{R}^\lambda$ from the Simple Ozone experiment. Solid line is an observed six-year monthly mean over Switzerland (from Dütsch, 1974).

experiment, but with a markedly higher amplitude. However, this seasonally varying chemistry-only calculation does not allow any systematic production of ozone because the values do not change from one year to the next.

The role of various atmospheric transport processes responsible for influencing the annual cycle of $\bar{R}^\lambda$ (48°N) is given in Eq. (5.1), which gives the zonal-mean ozone continuity equation in pressure coordinates:

$$\frac{\partial \bar{R}^\lambda}{\partial t} = -\underbrace{\frac{1}{a\cos\phi}\frac{\partial(\overline{v'R'}^\lambda \cos\phi)}{\partial\phi}}_{(E_H)} - \underbrace{\frac{\partial(\overline{\omega'R'}^\lambda)}{\partial p}}_{(E_V)} - \underbrace{\frac{\bar{v}^\lambda}{a}\frac{\partial\bar{R}^\lambda}{\partial\phi}}_{(M_H)} - \underbrace{\bar{\omega}^\lambda\frac{\partial\bar{R}^\lambda}{\partial p}}_{(M_V)}$$

$$+ \underbrace{\overline{\text{DIFFUSION}}^\lambda + \overline{\text{FILLING}}^\lambda}_{(DF)} + \underbrace{\overline{\text{SOURCES}}^\lambda - \overline{\text{SINKS}}^\lambda}_{(SMS)} + \underbrace{\overline{\text{RESIDUAL}}^\lambda}_{(RES)} \qquad (5.1)$$

The terms in Eq. (5.1) have the following physical contributions to the time rate of change of $\bar{R}^\lambda$ (net tendency):

(E_H) convergence of horizontal eddy tracer flux
(E_V) convergence of vertical eddy tracer flux
       horizontal advection of $\bar{R}^\lambda$ by the mean meridional circulation

(M_V) vertical advection of $\bar{R}^\lambda$ by the mean meridional circulation
(SMS) net of all non-conservative $\overline{\text{SOURCES}}^\lambda$ $- \overline{\text{SINKS}}^\lambda$ (see Sections 2b and 2c)
(DF) $\bar{R}^\lambda$ change due to the sum of $\overline{\text{DIFFUSION}}^\lambda$ and $\overline{\text{FILLING}}^\lambda$. (DIFFUSION represents the subgrid-scale flux due to the model's
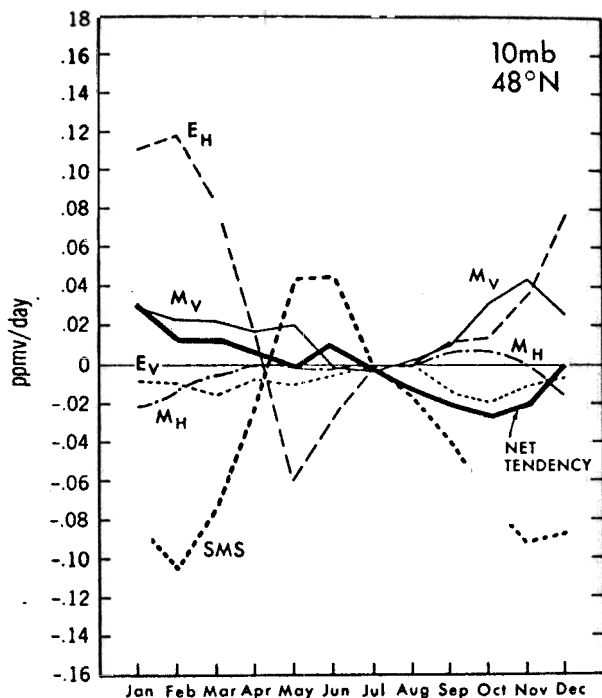
FIG. 5.2. Annual evolution of various contributions to the zonal-mean ozone balance (ppmv day^{-1}) computed at 10 mb, 48°N. Symbols are as given in Eq. (5.1).

nonlinear diffusion parameterization. FIL-LING is the mass conserving correction for the occasional negative mixing ratios that arise due to truncation error in the advection calculation. For details on these terms, see MM78.)

(RES) amount required to "correct" for the computational residual, or the accumulated imbalance in Eq. (5.1) due to errors arising from time sampling and interpolation from σ to p coordinates.

For the sake of brevity, the various processes will be referred to by the designators in parentheses. All terms are calculated by the accurate method described in Mahlman and Moxim (1976).

Fig. 5.2 shows the contribution of various terms in Eq. (5.1) to the zonal-mean ozone budget at 10 mb, 48°N for 12 months of the year. The positive tendency from January through April (see also Fig. 5.1) is dominated by E_H, with some assistance by M_V and strong opposition by SMS. Thus, even though the chemistry-only calculation of Fig. 5.1 predicts strong positive tendencies during this period, the full calculation of Fig. 5.2 shows net chemical destruction. This effect results from the net motions (particularly E_H) leading to $\bar{R}^\lambda$ values during this season which are consistently larger than that predicted by time-dependent local photochemistry. The strong E_H effect is due mainly to the dominant influence of the

quasi-stationary Aleutian anticyclone obtained in this dynamical simulation (see Fig. 10. of MM76 and Fig. 4.2 of MM78).

By May the tendency is near zero even though SMS is now positive, and M_V remains positive. This is because E_H becomes significantly negative due to the breakdown of the wintertime circulation as described in Mahlman (1973a) and MM78. In June this evacuation by E_H is much less. A positive tendency is produced which is related to net chemical production through SMS.

In August through November, the progressive lowering of the mean sun angle at 48°N leads to a significant net chemical destruction which appears directly responsible for the negative tendencies seen in Fig. 5.2. The influence of transport is to moderate this decrease through the combined positive contributions of M_V and E_H. Throughout the year, there is systematic removal of tracer to lower levels through E_V.

It is also of interest to view, at all latitudes, the ozone balances calculated from Eq. (5.1) at this same 10 mb level. Examples of such balances for six months of the year are given in Fig. 5.3. The September balances are dominated by ozone decreases in the Northern Hemisphere and increases in the Southern Hemisphere. In high northern latitudes, the circulation is marked by breakdown of the summer easterlies due to the decreased solar insolation. This leads to a positive E_H due to the waves in the forming westerlies. However, this effect is overbalanced by the strong chemical destruction at this time, as shown in Figs. 5.1 and 5.2. Equatorial latitudes are marked by a weak net photochemical production which is opposed mainly by E_H and M_V. High southern latitudes are dominated almost completely by strong ozone increases due to a positive SMS associated with a return of the sun to high latitudes.

Fig. 5.3 shows strongly different behavior during November. From about 40–70°N, moderate O_3 decreases are attributable to strong chemical destruction with rather complex net transport increases by mean cell and eddies in various combinations: near 60°N E_H, opposed by M_H; at 50°N $M_V + E_H$, opposed by E_V; near 35°N M_H, opposed by E_H and E_V. In high southern latitudes, SMS is acting mainly to compensate partially for the net transport which is dominated by eddy effects in various combinations.

Fig. 5.3 shows that by January the vigorous wintertime circulation of the model is acting to produce strong O_3 increases from about 35–65°N. This effect is due mainly to E_H with some contribution by E_V, while SMS is trying to destroy the excess as explained in the discussion for Fig. 5.2. In the subtropics, E_H and M_V are removing O_3, while M_H (advecting in higher equatorial values) and SMS are combining to balance the loss. In the 10°N–30°S

region, the net effect of the motions is to remove ozone efficiently. The primary process is M_V, which is acting to advect lower values of $\overline{R}^\lambda$ upward into the 10 mb level. This process has the effect of producing unrealistically small R values at 38 mb, while the very fast chemistry at this low latitude acts to keep the 10 mb R value large. The large vertical gradient subsequently produced leads to a simulated removal by E_V and DF. This noticeably large contribution of DF is an unrealistic computational byproduct of the large gradients of R between 10 and 38 mb leading to large horizontal gradients (which excite $\overline{\text{DIFFUSION}}^\lambda$ and negative mixing ratios at 38 mb (which excite $\overline{\text{FILLING}}^\lambda$). It is interesting to note that if ozone chemistry were included below 10 mb, this unrealistic effect would be greatly moderated. Thus, in this model it is difficult to ascertain whether the defect is one of transport or chemistry.[4] At high southern latitudes, the ozone is decreasing slightly because the chemical destruction is exceeding the weak increases due to the positive E_H remaining there during the summer period. This is a GCM defect relating to the model's undersimulation of the summer stratospheric easterlies in the Southern Hemisphere.

The March balances are quite similar to those of January except that the winter increase is displaced somewhat poleward. The equatorial removal by the net motions has diminished in intensity, thus reducing the magnitude of the production there as well. The removal at southern high latitudes is due basically to chemical destruction.

One very pronounced effect is the drastically differing "explanation" for the increases calculated for March northern latitudes, and the seasonal counterpart in September southern latitudes. In Southern Hemisphere September, the increase is dominated completely by chemistry, while in Northern Hemisphere March, the positive tendency is due to E_H. This provides an instructive example of the sensitivity of the chemistry to various aspects of the meteorological structure. The model Southern Hemisphere is characterized by relatively weak meridional O_3 transport, thus leading to a situation where the O_3 is below its chemical equilibrium value after the sun returns to the region. On the other hand, the model Northern Hemisphere region in March is characterized by strong meridional transfers and a resultant excess of O_3 over its local equilibrium value when the sun returns. However, this simple explanation is complicated considerably by the chemical sensitivity to temperature. At 60°N in March, the model zonal-mean temperature is 224 K, while at

60°S in September $\overline{T}^\lambda$ is 197 K. This difference leads to a situation where the time-dependent chemistry-only ozone mixing ratio is considerably less in the Northern Hemisphere for this case. Thus, at similar ozone values and sun angles, significant chemical destruction is occurring in the Northern Hemisphere near 60°N in March, while the opposite behavior is observed at 60°S in September. This striking interhemispheric asymmetry is related to the model's more active stationary planetary waves in the Northern Hemisphere (see MM76).

Fig. 5.3 shows the May balances to be dominated by the high northern latitudes exhibiting O_3 increases at the pole which are large enough to be opposed strongly by SMS. The net production in lower northern latitudes is opposed by E_H and M_V. In southern latitudes the buildup by M_V and E_H is overcome by chemical removal, leading to a small negative tendency.

In July the northern polar latitudes show removal by SMS with very weak transport effects. In low northern latitudes, E_V, E_H and M_V are all contributing to net removal, but are nearly balanced by SMS. In southern midlatitudes, the overall structure is qualitatively similar to its seasonal counterpart for the Northern Hemisphere in January. However, the magnitude of the January Northern Hemispheric effects is considerably larger (see also MM76).

b. 38 mb zonal-mean balances

The high correlation between the $\overline{R}^\lambda$ structure in the Stratified Tracer and Simple Ozone experiments demonstrates a marked insensitivity of the lower stratosphere horizontal tracer structure to significant differences in the mid-stratosphere. This result suggests that the 38 mb transport structure may be of considerable interest because of its role in these experiments as the first level below the region where the two experiments differ so drastically.

Examples of 38 mb balances for the two experiments are presented in Fig. 5.4 for January and July. For both months the net tendencies are remarkably similar in the two experiments. As pointed out for the previous experiment in MM78, the balances vary considerably from nearly complete self cancellation between mean cell and eddies in some cases, to strong tracer responses to particular transport processes in others. An interesting effect is that the magnitude of the various transport terms (and thus the degree of self cancellation) increases in the Stratified Tracer experiment with increasing latitude, especially in the winter hemisphere. Although a number of complex processes are operating, to a first approximation this difference results from the differences in the R value at 10 mb in the two experiments. The Stratified Tracer 10 mb constant value is scaled to be equal to the 10 mb average of the Simple Ozone experiment. Thus, the 10 mb mixing

---

[4] This effect is being examined independently with this model by a simulation of atmospheric N_2O (Levy et al., 1979), a tracer with substantially weaker chemistry in the equatorial middle stratosphere. Those results suggest that the defect of not including ozone chemistry at 38 mb provides the more serious difficulty.
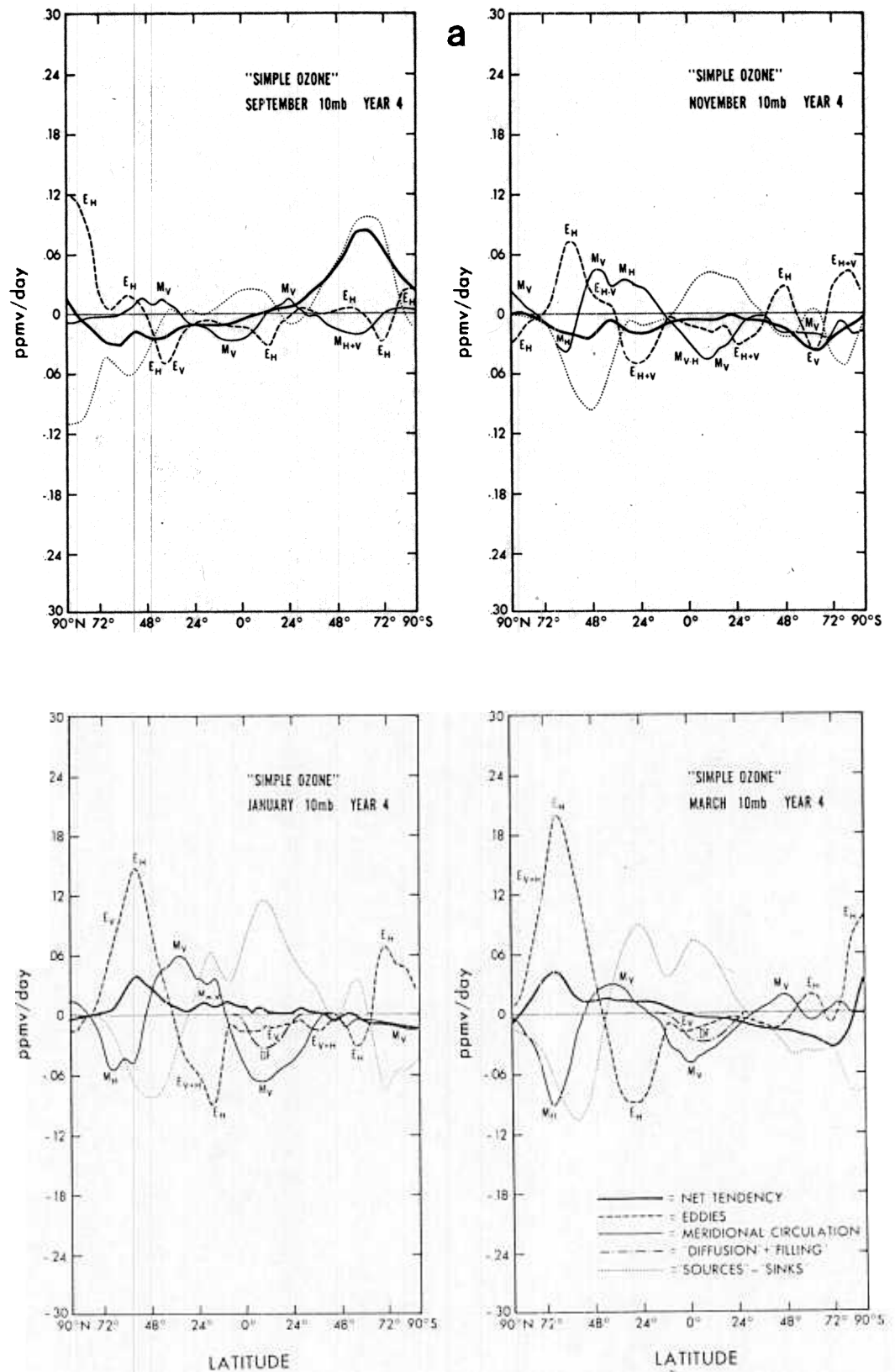
FIG. 5.3. 10 mb zonal-mean balances (ppmv day $^{-1}$) for indicated months from the Simple Ozone experiment. Symbols are as given in Eq. (5.1). The notations E_H, E_V, M_H or M_V mean that for the given mean (M) or eddy (E) contribution, either the vertical (V) or the horizontal (H) part dominates there as indicated.
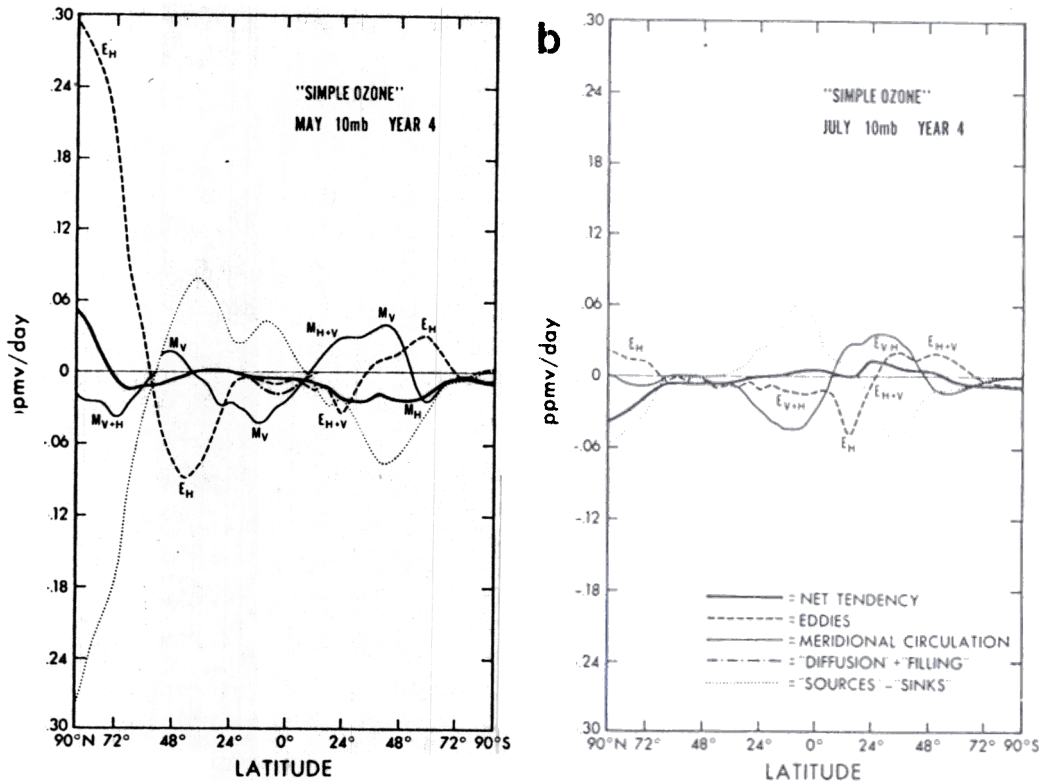
FIG. 5.3. (Continued)

ratio in the Simple Ozone experiment is small in high latitudes and large in low latitudes relative to the Stratified Tracer experiment. This is another way of pointing out that the average tracer values and how they change at a level tend to be related to the average stratification of the tracer rather than exhibiting a strong dependence upon local vertical gradients. This appears to be related to the qualitative validity (e.g., within a factor of 2 or so) of the one-dimensional vertical tracer diffusion models.

c. Approach to equilibrium

The results from the previous sections show that net chemical O_3 production or destruction in the middle stratosphere is strongly related to the motions there. In addition, the model's net destruction in the troposphere is dependent upon the transport rate to the troposphere as well as upon the tropospheric circulation itself. A relatively long time is required to move air parcels from the mid-stratosphere net source region to the troposphere destruction region. This implies that the time required for the stratospheric net source and tropospheric sink to come into a state of equilibrium is comparatively long. The processes by which this equilibration is approached are thus of considerable interest.

Fig. 5.5 shows the global average approach to equilibrium for the last three years of the Simple Ozone experiment. A striking feature is that the monthly mean stratospheric net SMS shows a pronounced seasonal dependence. A maximum net source is present in January–February with a lesser peak in August–September. A surprising feature is that net stratospheric ozone destruction appears in several months, with the largest sinks appearing in November and May. Analysis of the 10 mb ozone balances as seen in Fig. 5.3 shows that the months with large net sources are dominated by large O_3 flux convergences at higher latitudes of the winter hemisphere. The difference in the magnitude of the peaks is due to the stronger winter poleward O_3 flux in the model Northern Hemisphere noted earlier. The March and November net stratospheric sinks are more complex but are largely associated with model photochemical losses excited by an autumnal departure of the sun from the summer hemisphere.

The tropospheric destruction in Fig. 5.5 shows a much smaller seasonal dependence. The 12-month average net SMS, obtained by adding the stratospheric SMS and tropospheric SMS, shows a rather smooth asymptotic approach to equilibrium (net SMS = 0). The e-folding time of this approach to equilibrium is about 11 months. This value is related to the average time required for air to move to the sink region from the lower boundary of the net source region.

d. Mechanisms leading to the poleward-downward slope of $\bar{R}^\lambda$ surfaces

One of the useful features of the design of the Stratified Tracer experiment is that its initial condi-
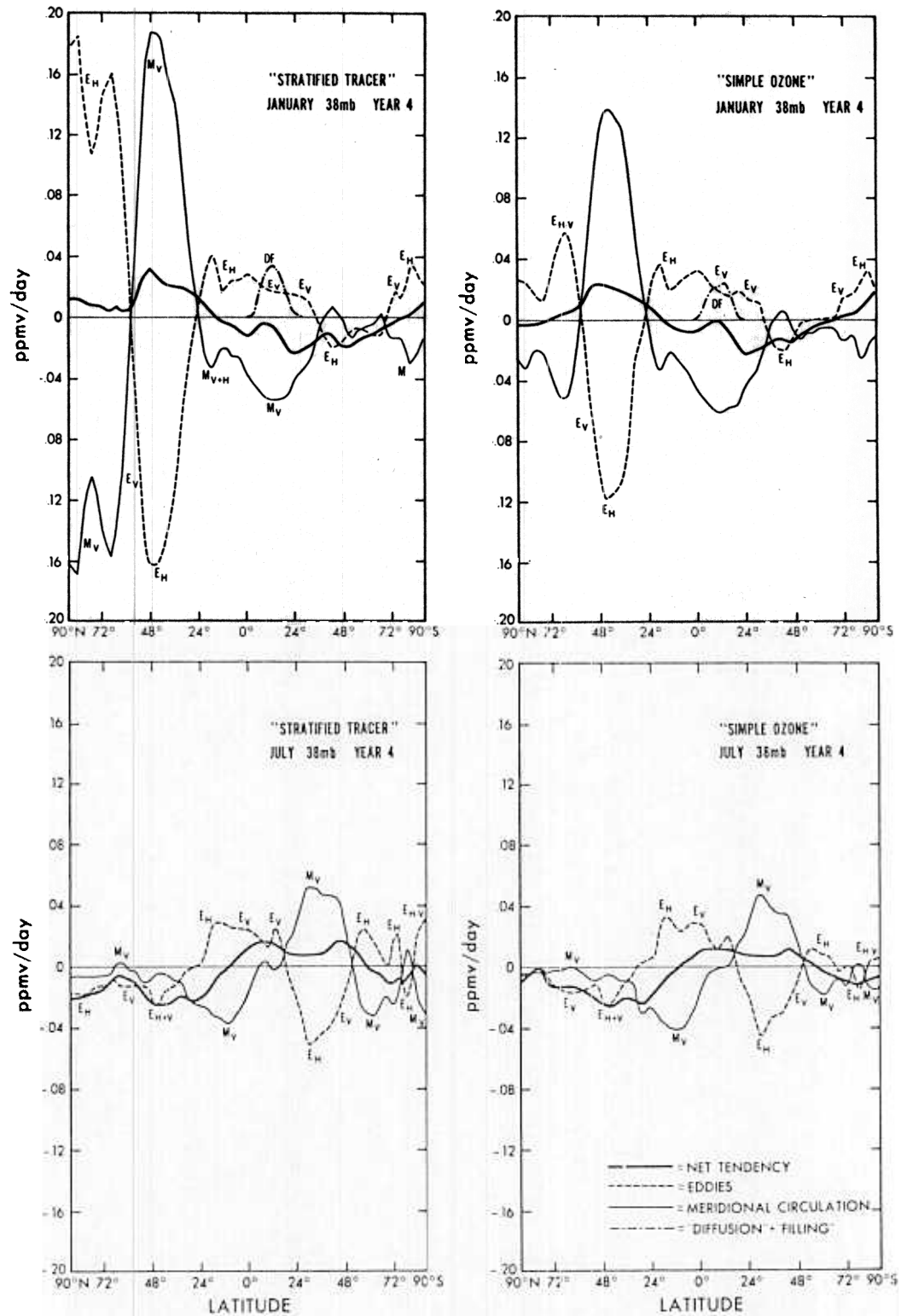
FIG. 5.4. 38 mb zonal-mean balances (ppmv day^{-1}) for January and July from the Simple Ozone and Stratified Tracer experiments as indicated. Symbols as given in Eq. (5.1).

tion contains no horizontal tracer gradients on isobaric surfaces. It is thus of considerable interest to examine the processes by which the $\bar{R}^{\lambda}$ distribution evolves rapidly into the rather steep meridional tracer gradients seen in Fig. 3.2a for October year 1.

An important feature of this experiment and the

one reported in MM78 is that the normally large degree of self cancellation between mean cell and eddy transports (e.g., see Fig. 5.4) is not really present in the earliest stages of an experiment. This is partly because the tracer has not yet had time to become well distributed relative to the large-scale disturbances present. Thus, for an initial period of time, various zonal-mean and eddy tracer transport processes tend to operate more independently of one another.

The evolution of the meridional slope of $\bar{R}^{\lambda}[\partial(\partial z/\partial y)_{\bar{R}^{\lambda}}/\partial t]$ proceeds in the first stages of this experiment at the rate of about -5.5×10^{-4} month^{-1}. This is a surprisingly large fraction of the long-term average slope of about -8×10^{-4} as obtainable from Fig. 3.2b.

A way to investigate the physical processes leading to this pronounced change in tracer slope is to evaluate the operative terms in the equation for the rate of change of tracer slope, i.e.,

$$\frac{\partial}{\partial t}\left(\frac{\partial z}{\partial y}\right)_{\bar{R}^{\lambda}}$$

$$= \frac{\partial}{\partial t}\left(-\frac{\dfrac{\partial \bar{R}^{\lambda}}{\partial y}}{\dfrac{\partial \bar{R}^{\lambda}}{\partial z}}\right)$$

$$\frac{1}{\dfrac{\partial \bar{R}^{\lambda}}{\partial z}}\left[\frac{\partial}{\partial y}\frac{\partial \bar{R}^{\lambda}}{\partial t}+\left(\frac{\partial z}{\partial y}\right)_{\bar{R}^{\lambda}}\frac{\partial}{\partial z}\frac{\partial \bar{R}^{\lambda}}{\partial t}\right]$$

Because the interest here is to understand the early evolution of this experiment, substantial simplifications are possible. At the onset of the experiment, $(\partial z/\partial y)_{\bar{R}^{\lambda}} = 0$ everywhere. Also $\partial\bar{R}^{\lambda}/\partial z = (\partial R/\partial z)_{t=0}$ everywhere. With these specifications, upon substitution of Eq. (5.1), Eq. (5.2) becomes

$$\frac{\partial}{\partial t}\left(\frac{\partial z}{\partial y}\right)_{\bar{R}^{\lambda}} \approx -\frac{1}{\left(\dfrac{\partial R}{\partial z}\right)_{t=0}}$$

$$\times \frac{\partial}{\partial y}\,[E_H + E_V + M_V + \text{smaller terms}], \quad (5.3)$$

where the symbols E_H, E_V and M_V carry the meanings given in Eq. (5.1) (M_H is small because $\partial\bar{R}^{\lambda}/\partial y = 0$ initially).

In looking at the problem of net tracer dispersion in the stratosphere, a view of the system in isentropic coordinates (e.g., Danielsen, 1968) makes it clear that irreversible vertical transfer on time scales longer than a year depends upon the existence of diabatic processes. However, what remains unclear is just how those necessary diabatic processes interact with the adiabatic processes to produce the observed transport behavior. This approach has re-
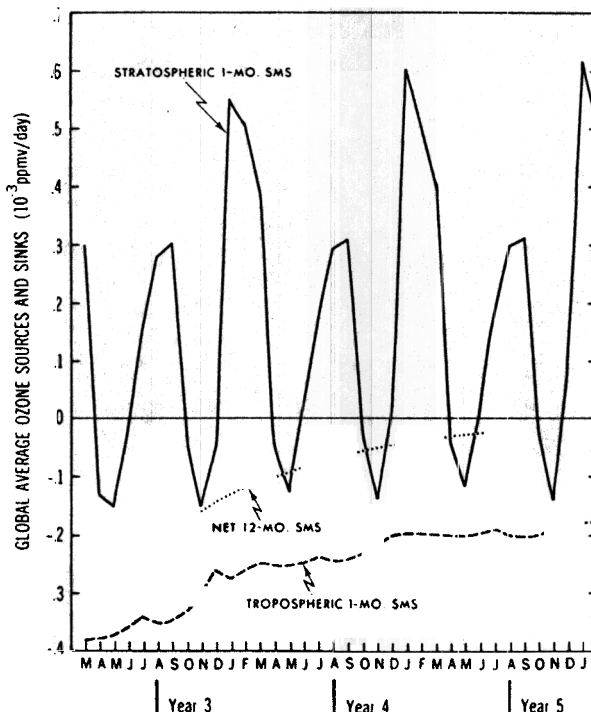

FIG. 5.5. Global average sources and sinks (10^{-3} ppmv day^{-1}) from the Simple Ozone experiment. Solid lines show stratospheric monthly mean net SMS averaged over the entire atmosphere. Dashed lines give monthly mean tropospheric destruction. The dotted line is the 12-month running mean of the net atmospheric SMS.

ceived renewed emphasis by Matsuno,[5] Andrews and McIntyre (1976), Kida (1977a,b) and Dunkerton (1978) through the so-called Lagrangian-mean viewpoint on atmospheric dynamics. Matsuno, Kida, and Dunkerton all emphasized the importance of the zonal-mean diabatic circulation (e.g., Murgatroyd and Singleton, 1961) in preference to the actual meridional circulation. It thus is of considerable interest to examine the relative importance of this effect on the rapid evolution of poleward-downward $\bar{R}^{\lambda}$ surfaces in this experiment.

To introduce the effect of the zonal-mean diabatic circulation, a manipulation of the M_V term in Eq. (5.3) is required:

$$M_V = -\bar{\omega}^{\lambda}\frac{\partial\bar{R}^{\lambda}}{\partial p} \approx -\bar{w}^{\lambda}\frac{\partial\bar{R}^{\lambda}}{\partial z}$$

$$= -\bar{w}^{\lambda}_d\cdot\frac{\partial\bar{R}^{\lambda}}{\partial z} - \bar{w}^{\lambda}_{ad}\frac{\partial\bar{R}^{\lambda}}{\partial z}$$

where w_{ad} and w_d are the adiabatic and diabatic parts of the vertical velocity, respectively, expressed in approximate (and somewhat arbitrary) form as

[5] Matsuno, T., 1972: Paper presented at CIAP Workshop on Computational Modeling of the Atmosphere, Pacific Grove, CA.

$$w_{ad} \approx \frac{-\frac{\partial T}{\partial t} - u\frac{\partial T}{\partial x} - v\frac{\partial T}{\partial y}}{\frac{g}{c_p} + \frac{\partial T}{\partial z}},$$

$$w_d \approx \frac{Q/c_p}{\frac{g}{c_p} + \frac{\partial T}{\partial z}},$$

where Q is the diabatic heating rate, g the acceleration of gravity and c_p the specific heat at constant pressure. Using the above substitutions, Eq. (5.3) becomes

$$\frac{\partial}{\partial t}\left(\frac{\partial z}{\partial y}\right)_{\bar{r}^\lambda} \approx \frac{\partial \bar{w}_d^\lambda}{\partial y} + \frac{\partial \bar{w}_{ad}^\lambda}{\partial y} - \frac{1}{\left(\frac{\partial R}{\partial z}\right)_{t=0}}\frac{\partial}{\partial y}E_H$$

$$- \frac{1}{\left(\frac{\partial R}{\partial z}\right)_{t=0}}\frac{\partial}{\partial y}[E_V + \text{smaller terms}]. \quad (5.4)$$

In this form the importance of the zonal-mean diabatic circulation can be evaluated relative to the other terms in Eq. (5.4). For the parent GCM used in this tracer model (MM76), characteristic zonal-mean diabatic heating rates at 110 mb for August are about $+0.3°C$ day^{-1} in low latitudes and $-0.3°C$ day^{-1} in high northern latitudes. Thus the $\partial \bar{w}_d^\lambda/\partial y$ term in Eq. (5.4) produces a systematic change in the meridional tracer slope of about -1.8×10^{-4} month^{-1}.

The $\partial \bar{w}_{ad}^\lambda/\partial y$ term offers little systematic contribution to the average slope increase because it is composed of alternating algebraic signs along the meridian (see MM76). Its overall effect is to flatten the slope because of the tendency for rising motion at the pole. Also, even at this early stage, there is some tendency for the M_V and E_H terms to cancel. (At 110 mb M_V and E_H show a -0.4 correlation.)

The third term on the right-hand side of Eq. (5.4) exhibits a systematic effect on the tracer slope. As shown in Mahlman (1973a), the initial stages of this experiment are marked by strong poleward eddy flux producing an evacuation of tracer at 110 mb in equatorial regions and a buildup at high latitudes. The magnitude of this effect in Eq. (5.4) is about -0.5×10^{-4} month^{-1}.

The fourth term on the right-hand side of Eq. (5.4) is highly significant because a pronounced removal due to E_V is occurring in low latitudes, while very little contribution due to E_V is present at high latitudes. This effect alone produces a slope change of about -3.5×10^{-4} month^{-1}. The dominance of this term is related to the greater depth of the troposphere in low latitudes with its attendant lower static stability and large local vertical velocities (relative to values at 110 mb in middle and high latitudes).

Note that in this term the diabatic and adiabatic vertical velocities have not been separated. However, the diabatic part of this term should contribute strongly because of the rapid systematic tracer movement relative to the nearly stationary isentropic surfaces near the tropical tropopause region (see Fig. 3.2).

The sum of the above processes leads to a predicted slope change of -5.8×10^{-4} month^{-1} versus an observed change of -5.5×10^{-4} month^{-1}. The weak slope-increasing contribution of the $\partial \bar{w}_{ad}^\lambda/\partial y$ term leads to a condition of near balance for Eq. (5.4) without inclusion of the smaller terms.

The dominance of the vertical eddy flux convergence term in Eq. (5.4) leads to an important question as to the relative importance of the contribution of the diabatic vertical eddy velocity in producing poleward-downward slopes of tracer isopleths. This is especially so in view of the above demonstrated importance of the $\partial \bar{w}_d^\lambda/\partial y$ term. In the above analysis, it has not been possible to separate out the diabatic eddy vertical velocity directly because of the specialized analysis scheme required to achieve an unambiguous transformation from sigma to pressure coordinates (Mahlman and Moxim, 1976).

An alternative analysis approach, however, can yield some insight into the relative importance of the eddy diabatic effects toward producing the strong poleward-downward slope of mixing ratio isopleths. Consider the equation of eddy temperature expressed in the approximate form

$$\frac{\partial T'}{\partial t} = -\bar{u}^\lambda\frac{\partial T'}{\partial x} - \bar{v}^\lambda\frac{\partial T'}{\partial y} - v'\frac{\partial \bar{T}^\lambda}{\partial y}$$

$$- \bar{w}^\lambda\frac{\partial T'}{\partial z} - w'\left(\frac{g}{c_p} + \frac{\partial \bar{T}^\lambda}{\partial z}\right)$$

$$+ \frac{Q'}{c_p} + \text{higher order terms (h.o.t.).} \quad (5.5)$$

Although Eq. (5.5) is actually expressed on a pressure surface, the term $\omega\alpha$ has been replaced by $-gw$ to simplify the physical interpretation of the final form. If Eq. (5.5) is multiplied by T' and zonally averaged, one obtains an eddy temperature variance equation

$$\frac{\partial}{\partial t}\frac{\overline{T'^2}^\lambda}{2} = -\overline{v'T'}^\lambda\frac{\partial \bar{T}^\lambda}{\partial y} - \overline{w'T'}^\lambda\left(\frac{g}{c_p} + \frac{\partial \bar{T}^\lambda}{\partial z}\right)$$

$$+ \frac{\overline{Q'T'}^\lambda}{c_p} - \bar{v}^\lambda\frac{\partial}{\partial y}\frac{\overline{T'^2}^\lambda}{2}$$

$$- \bar{w}^\lambda\frac{\partial}{\partial z}\frac{\overline{T'^2}^\lambda}{2} + \text{h.o.t} \quad (5.6)$$

Rearrangement of Eq. (5.6), noting the definition of potential temperature and that $\partial z/\partial y_\theta = -\partial\theta/\partial y/$

$\partial\theta/\partial z$, gives for an "eddy mixing slope"

$$\frac{\overline{w'T'}^\lambda}{\overline{v'T'}^\lambda} = \frac{\partial z}{\partial y_\theta} + \frac{\overline{Q'T'}^\lambda}{c_p \overline{v'T'}^\lambda \left(\dfrac{g}{c_p} + \dfrac{\partial \overline{T}^\lambda}{\partial z}\right)} \qquad \frac{\left(\dfrac{\partial}{\partial t}\dfrac{\overline{T'^{2}}^\lambda}{2} + \bar{v}^\lambda \dfrac{\partial}{\partial y}\dfrac{\overline{T'^{2}}^\lambda}{2} + \bar{w}^\lambda \dfrac{\partial}{\partial z}\dfrac{\overline{T'^{2}}^\lambda}{2}\right) + \text{h.o.t.}}{\overline{v'T'}^\lambda \left(\dfrac{g}{c_p} + \dfrac{\partial \overline{T}^\lambda}{\partial z}\right)}$$

This equation states physically that for linear, steady, adiabatic eddy motion, the average meridional eddy mixing slope of air will remain constrained to its appropriate zonal-mean isentropic surface. Alternatively, this would imply no systematic production of $\overline{T'^2}^\lambda/2$ by eddy motions acting on mean gradients. However, removal of any of these constraints allows eddy fluxes across the zonal-mean isentropic surface. This is important because, as pointed out by Hering (1965) and MM78 (for this model), the meridional slopes of potential vorticity and tracer surfaces in the lower stratosphere are significantly steeper than those of isentropic surfaces.

For this GCM the value of the $\partial z/\partial y_\theta$ term on the right-hand side of Eq. (5.7) is about -3×10^{-4}, a value (at equilibrium) which is smaller than the initial one month change in the slope of the $\overline{R}^\lambda$ surface. However, the second term on the right-hand side of Eq. (5.7) from the GCM has a value of about -2×10^{-4}. This results from the systematic relative diabatic cooling of sinking warm air and heating of ascending cold air in the presence of a poleward eddy heat flux (which provides for a dissipation of $\overline{T'^2}^\lambda/2$). This process thus contributes significantly toward explaining the observation that quasi-conservative tracers exhibit steeper meridional slopes than do isentropic surfaces. The remaining terms in Eq. (5.7) can be significant in localized circumstances, but generally appear to be of lesser importance than the first two terms.

A further interesting aspect of the implications of Eq. (5.7) is that tracers can be expected to be transported by the eddies poleward and downward relative to the mean isentropic surfaces, as long as the eddy heat flux is directed poleward. This should be the case even when $\partial z/\partial y_\theta$ is positive. Some related aspects of this transport problem were addressed by Wallace (1978).

e. Some aspects of Lagrangian interpretation of transport in stationary planetary waves

As mentioned in the previous section, the so-called Lagrangian-mean perspective is being increasingly recognized as an important means of providing simplifying interpretations of various transport phenomena. A number of earlier studies invoked rather similar reasoning processes toward understanding specific (rather than zonal-mean) processes such as annulus flows (Riehl and Fultz, 1957), the subtropical jet stream (Krishnamurti, 1961), the t jet stream (Danielsen, 1968; Mahlman,

1973b) and the stratospheric polar night vortex (Mahlman, 1969). Except for the subtropical jet stream, in each of the other problems, a local thermodynamically direct circulation was identified which is opposite in sense to the corresponding mean meridional circulation.

It thus is of considerable interest that the concept of Lagrangian-mean dynamics has been advanced recently through the work of Matsuno,[5] Andrews and McIntyre (1976, 1978a,b), Kida (1977b), Dunkerton (1978) and Matsuno and Nakamura (1979). This type of work suggests that much of the mystery of the near cancellation of mean cell and eddy transports of conservative tracers can be resolved by employing such a Lagrangian perspective.

An attractive possibility is to employ such a Lagrangian-type approach to the analysis of this tracer experiment. However, for long-term processes a disadvantage of this approach becomes immediately evident. In the presence of the moderately strong wind deformation in the stratosphere, an individual fluid parcel becomes "stretched out" quickly to the place that its individual position becomes very difficult to define. In addition, the definition of an appropriate coordinate averaging axis for viewing Lagrangian motion can be rather arbitrary and makes it difficult to perform accurate calculations. Nevertheless, the qualitative insights gained through such a procedure can be sufficient to overcome these disadvantages.

Before actual calculations are presented, it is appropriate to look at some simple theoretical considerations relevant to this problem. The works of Eliassen and Palm (1960) and Charney and Drazin (1961) first presented theoretical arguments which pointed out that, under a number of restrictions, waves do not necessarily lead to systematic acceleration of zonal flows. These results were generalized by Dickinson (1969), Holton (1974), Boyd (1976) and Andrews and McIntyre (1976, 1978b) for progressively less restrictive circumstances. The above results may also prove to be quite useful for understanding the processes which act to disperse trace constituents.

In this section, an alternative perspective will be developed on the same type of problem mentioned above, but oriented toward improvement of understanding of the tracer behavior simulated in this model.

For the hydrostatic, "primitive" equations system, the energy equation expressed in isentropic

coordinates can be written as

$$\frac{dM}{dt_\theta} + \underset{(a)}{\frac{d(V_s^2/2)}{dt_\theta}} = \underset{(b)}{\frac{\partial M}{\partial t_\theta}} - \underset{(c)}{\frac{d\theta}{dt}\frac{\partial(V_s^2/2)}{\partial\theta}} + V_2 \cdot F, \quad (5.8)$$

where M is the Montgomery streamfunction $(c_pT + \phi)$, V_s the total horizontal wind speed, $V_2 \cdot F$ the local kinetic energy dissipation and ϕ the geopotential (Danielsen, 1961). Here the θ subscript indicates that the substantial and partial derivatives are evaluated on an isentropic surface as indicated. Also, note that in this problem, the usual substantial derivative is defined as

$$\frac{D(\quad)}{Dt} = \frac{d(\quad)}{dt_\theta} + \frac{d\theta}{dt}\frac{\partial(\quad)}{\partial\theta}.$$

$$\frac{d(\quad)}{dt_\theta} = \frac{\partial(\quad)}{\partial t_\theta} + V_2 \cdot \nabla_\theta(\quad),$$

where V_2 is the horizontal wind vector and ∇_θ is the two-dimensional gradient operator evaluated on an isentropic surface.

Following Danielsen (1961), if Eq. (5.8) is integrated in time following the projection of a particle onto the original isentropic surface from its beginning position (b) to its final position (F), the statement of balance is[6]

$$(M + V_s^2/2)_\theta|_{t_F} - (M + V_s^2/2)_\theta|_{t_b} = \underset{(a)}{\int_{t_b}^{t_F}\frac{\partial M}{\partial t_\theta}dt}$$

$$\underset{(b)}{- \int_{\theta_b}^{\theta_F}\frac{\partial}{\partial\theta}V_s^2/2\,d\theta} + \underset{(c)}{\int_{t_b}^{t_F}V_2 \cdot F\,dt}. \quad (5.9)$$

Eq. (5.9) states that if the mass field is locally steady along the trajectory path (term a), adiabatic (term b) and frictionless (term c), the quantity $M + V_s^2/2$ is conserved following the particle. These are similar, but not identical to the more fundamental conditions satisfying the nonacceleration theorems mentioned above. If these three conditions are satisfied, the particle will move along isopleths of $M + V_s^2/2$. If the distribution of $M + V_s^2/2$ is such that there always exists a gradient normal to the trajectory, a particle will return to *exactly* its original latitude on returning to its original longitude after one orbit around the earth. Thus, no net transport or net par-

---

[6] Note that the integration in Eq. (5.9) is with respect to the path of a single particle. Thus, in many circumstances, it differs from the generalized Lagrangian-mean description of Andrews and McIntyre (1976, 1978a,b) and Matsuno and Nakamura (1979) which refer to an average along a "material tube" of fluid particles. However, in the case of steady, frictionless, adiabatic motion, an isopleth of $M + V_s^2/2$ on an isentropic surface should normally correspond to an appropriate "material tube."

ticle acceleration will have occurred (under these three assumptions), in the sense that systematic particle movement relative to a stationary mass field is not allowed as long as $\partial(M + V_s^2/2)/\partial n_\theta$ is monotonic (n is the coordinate direction normal to the trajectory). The conditions under which this is not satisfied can be seen by performing the indicated differentiation and separating V_s into its ageostrophic (ag) and geostrophic (g) parts

$$\frac{\partial}{\partial n}(M + V_s^2/2)_\theta = -f\left[V_s(g)\left(1 - f^{-1}\frac{\partial V_s}{\partial n_\theta}\right.\right.$$
$$\left.\left. - f^{-1}V_s(ag)\frac{\partial V_s}{\partial n_\theta}\right].\quad (5.10)$$

The above quantity is virtually always negative in the stratosphere in view of the approximately geostrophic character of the motions. An exception can occur when an anticyclonic wind shear on an isentropic surface exceeds the local Coriolis parameter. This is the usual condition for inertial instability (normally associated with nonsteady conditions). Its occurrence thus could lead to enhanced local tracer dispersion. Another perspective is that the right-hand side of Eq. (5.10) is always negative, except possibly when the Rossby number is of order one or greater.

In the above analysis, it can also be seen that no *systematic* transport across $M + V_s^2/2$ lines should occur for the case of adiabatic, dissipation-free, linear propagating disturbances. For any set of disturbances and phase speeds under these assumptions, a particle will eventually return to its original position after an arbitrarily large number of orbits. Thus, no *systematic* transport will have occurred.

It is of interest to point out what type of response such a "nontransport" idealized situation would show for a local injection of inert tracer when viewed from the "traditional" perspective of zonal-mean balances on pressure surfaces [Eq. (5.1)]. Immediately, a drastic change in $\overline{R}^\lambda$ would occur due to E_H. (For infinitesimal disturbance amplitude, nothing would happen to $\overline{R}^\lambda$.) Within about two weeks, the zonal-mean tendency $(\partial\overline{R}^\lambda/\partial t)$ would decrease appreciably in magnitude. After a month or two, the tendency would be nearly zero and exhibit a pronounced cancellation between mean cell and eddy transport effects, typically between E_H and M_V. From the Lagrangian perspective, however, the tracer would have been merely "stringing out" along constant $M + V_s^2/2$ lines on the isentropic surface, with no systematic transfer occurring normal to those lines.

Such a scenario describes rather well the $\overline{R}^\lambda$ behavior in the first month of the instantaneous source experiment described in MM78 (see also Hunt and Manabe, 1968). Over longer periods, however, the MM78 experiment shows considerably
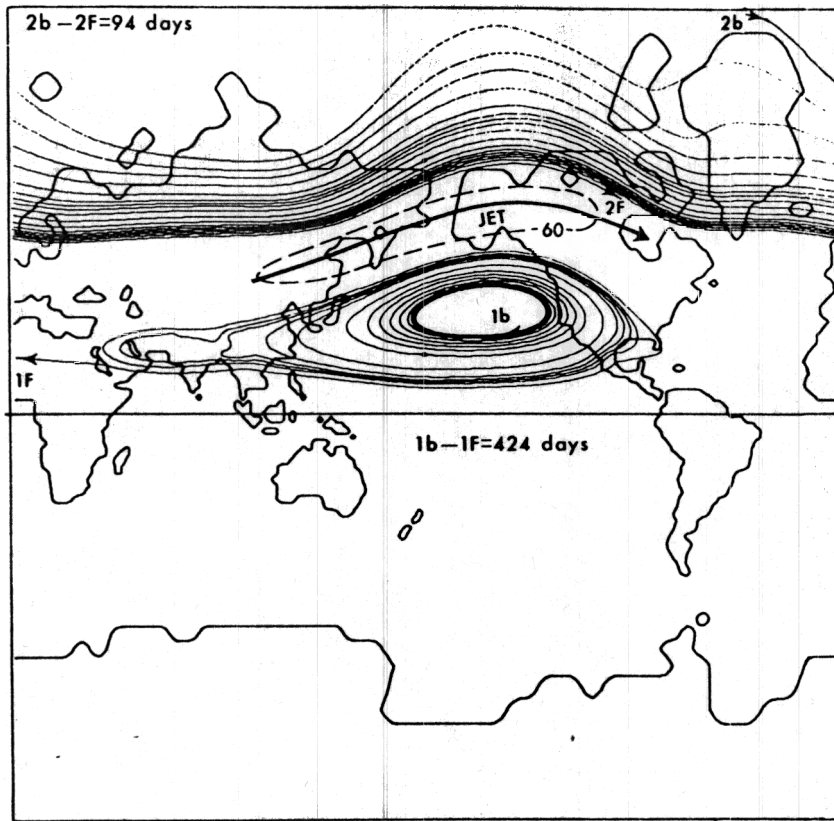
JANUARY 38mb

FIG. 5.6. Isobaric movement of two particles in the GCM for the 38 mb January-mean flow. Note poleward drift out of Aleutian high and into the time-mean jet stream axis of particle No. 1 and equatorward drift of particle No. 2. The dashed line is the 60 m s⁻¹ isotach of the January-mean flow.

different behavior from that in the above simple picture. This is because of the very significant effects which occur due to the relaxation of the constraints on the right-hand side of Eq. (5.9).

As a preliminary step toward analysis of this experiment from a Lagrangian perspective, a calculation of horizontal particle drift for very special circumstances has been made. In view of the stationarity assumption required in Eq. (5.9) to get closed orbit trajectories, this first calculation determines the particle movement in the January-averaged flow. This calculation thus does not necessarily produce the same net particle movement that would be obtained in the complete three-dimensional time-dependent flow. Nevertheless, this portion of the total particle movement is of considerable intrinsic interest in view of the relatively strong stationarity of the wintertime stratospheric flow. In addition, it is of interest to establish the importance of the particle movement in the time-mean flow relative to the total particle movement.

To accomplish this calculation, particles are introduced into selected locations at various isobaric levels for the January-mean flow in the GCM. These particles are followed *isobarically* for long enough periods that the sense of mean drift can be completely established at each level. The structure of the January-mean flow for this model is given in MM76 and MM78. Basically it shows that the flow is dominated by the Japan jet in the upper troposphere which merges with and produces a strong Aleutian anticyclone in the stratosphere.

An example of the movement of two particles in this mean flow is shown in Fig. 5.6 for the 38 mb level. This figure shows that the particles are drifting into the jet stream region from both sides. This drift is thus quite different from the drift due to the Eulerian-mean diabatic circulation discussed in Section 5d, which implies poleward motion everywhere at this level. The sense of this drift is somewhat similar to the meridional circulation presented for this GCM in Fig. 5.1 of MM76. However, the line of convergence for this mean drift is considerably poleward of that of the mean meridional circulation. In addition, the magnitude of the drift shown in Fig. 5.6 is ~ 0.15 m s⁻¹ (compared to the 60 m s⁻¹ basic speed of the jet itself). The corresponding $\bar{v}^{\lambda}$ in the same region at 38 mb is $\sim 0.35 - 0.40$ m s⁻¹.

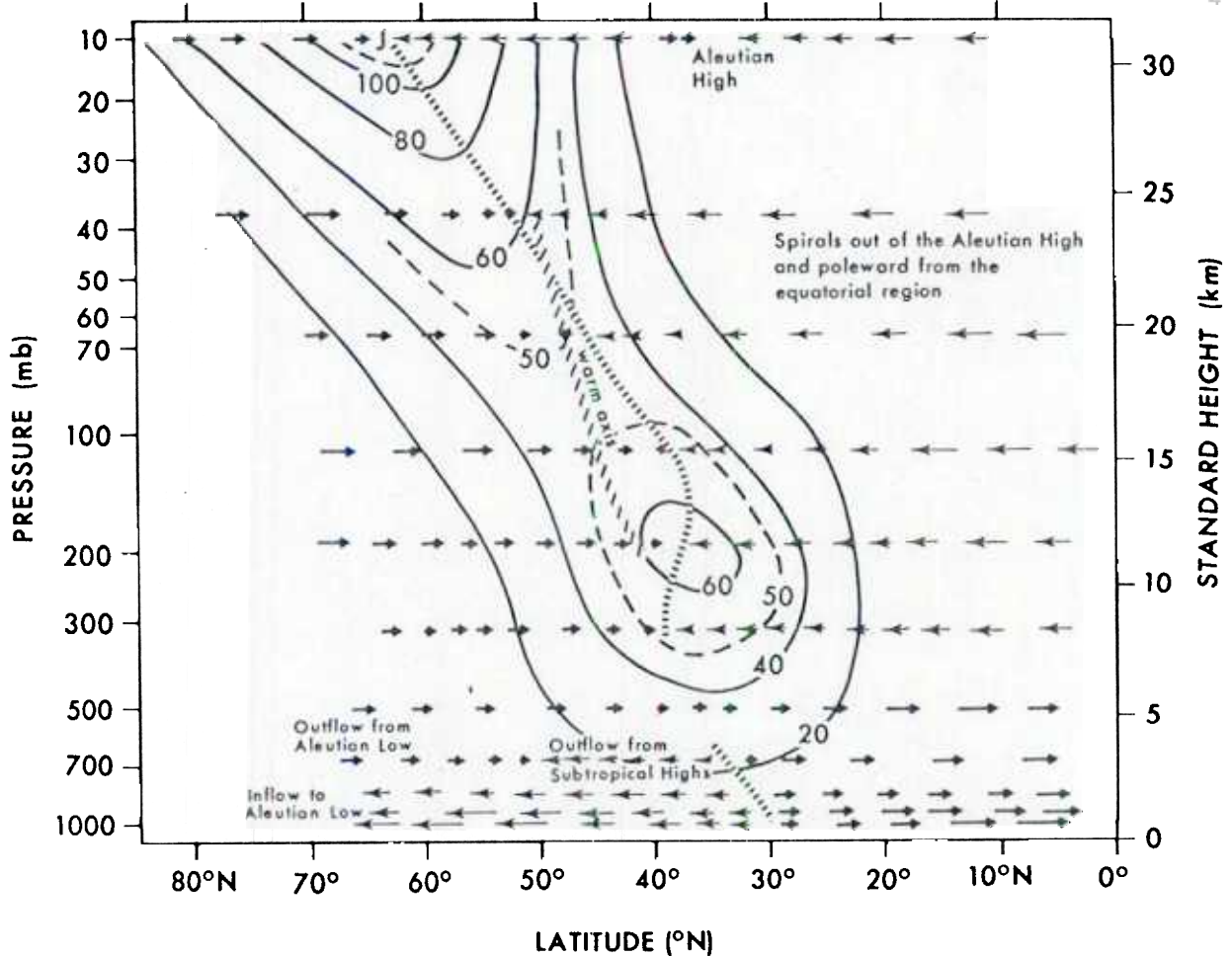Qualitative view of net particle drift relative to simulated January-mean jet stream. (No mean-cell eddy separation)

FIG. 5.7. Schematic view of net drift of all particles in the January-mean flow. Solid lines are isotachs (m s⁻¹) at 150°E. Horizontal drift speed is roughly proportional to length of arrows. Actual drift is relative to time-mean flow axis, not latitude (see Fig. 5.6). Note position of strong convergence of particles (dashed lines) at and to the poleward side of the time-mean jet stream axis. The axis of warmest air is given by the diagonal dashed line.

A schematic view of the particle drift in the time-mean flow is given in Fig. 5.7 and is shown as drift relative to the strong jet stream structure present at 150°E (see Fig. 10.5 of MM76). The most remarkable characteristic is that the drift in this mean flow is essentially into the isotach maximum at all levels. The length of the arrows is approximately proportional to the strength of the transverse drift. It is interesting that the point of maximum *convergence* of drift tends to be near the axis of warmest air as indicated in Fig. 5.7 (see also Fig. 5.10 in MM76). Note that in the lower troposphere, the pattern of drift is quite different. It is dominated by mean outflow from the subtropical anticyclones and flow into the Aleutian low. Higher up, the stationary flow is out of the Aleutian low at all levels as it merges continuously into the polar night vortex (as viewed in the time-mean flow).

The influence of the mean drift shown in Fig. 5.7 on the tracer field in these experiments is shown in Fig. 5.8. This figure portrays the time-averaged tracer field from the Stratified Tracer experiment for January in the first year of the experiment. The tracer values are averaged at 150°E, as this is a region where the stationary flow is reasonably zonal. However, this tracer structure is reasonably similar to the distribution normal to this time-mean flow at other longitudes as well.

The most notable feature of Fig. 5.8 is that the tracer field shows strong gradients across the jet axis, with a maximum just on the cyclonic shear side of the jet axis. This type of distribution is quite

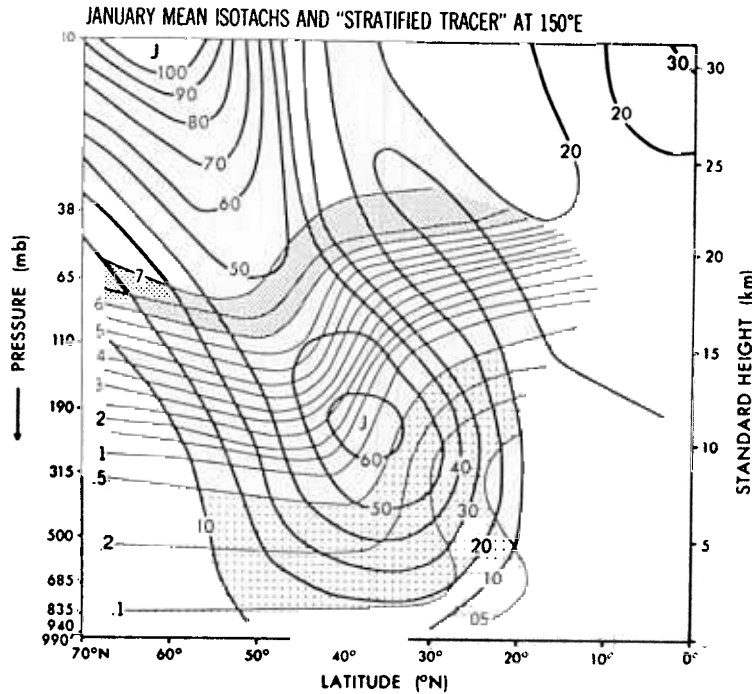JANUARY MEAN ISOTACHS AND "STRATIFIED TRACER" AT 150°E

FIG. 5.8. January-mean mixing ratio from year 1 of the Stratified Tracer experiment calculated relative to the strong stationary jet stream at 150°E. Note high values on the poleward side of the jet stream axis.

consistent with the mean drift structure shown in Fig. 5.6. It is also consistent with the schematic picture reported by Danielsen (1968), and the dynamically computed transverse circulation about the polar front jet stream presented by Mahlman (1973b). In addition, it is consistent with observations of trace constituents (e.g., Lovill, 1974). Another point of interest is that this region of tracer maximum in Fig. 5.8 corresponds rather closely with the positive $\bar{R}^\lambda$ tendency for 38 mb seen near 50°N in Fig. 5.4 (see also Fig. 5.12 in MM78). In Fig. 5.4 this increase in $\bar{R}^\lambda$ is "explained" by a positive M_V being slightly larger than the tracer removal by E_V and E_H. (For a similar perspective on the "explanation" of the mid-latitude warm belt, see MM76, Section 10.) Thus, in this case of large apparent cancellation between mean cell and eddy transports, the interpretation can become less complex through adoption of a Lagrangian-type perspective.

In spite of the apparent success of the simplifying perspective of the above arguments, this type of mean drift is not sufficient to explain all aspects of simulated and observed tracer behavior. For example, the model shows a pronounced long-term tendency to exhibit high mixing ratios within the polar vortex itself, particularly in non-winter seasons. Some insight on the limitation of the mean flow drift perspective offered above can be gained by consideration of the heat balance of the region

bounded by the line of convergence of mean drift as illustrated in Figs. 5.6 and 5.7. If the first law of thermodynamics is averaged over this region, the appropriate expression is

$$\frac{\partial \tilde{T}}{\partial t} = A^{-1} \oint \bar{C}_n^B (\bar{T}^B - \tilde{T}) \delta l$$

$$+ A^{-1} \oint C_n'' T'' \delta l + \tilde{\omega} \left(\frac{\tilde{\alpha}}{c_p} - \frac{\partial \tilde{T}}{\partial p} \right)$$

$$- \frac{\partial}{\partial p} \widetilde{\omega^* T^*} + \frac{\widetilde{\omega^* \alpha^*}}{c_p} + \frac{\tilde{Q}}{c_p} , \quad (5.11)$$

where ($\tilde{\ }$) is an average over the specified area, ($\bar{\ }$)^B an average along the lateral boundary to that area, ( )$'' = ( ) - (\ )^B$, ( )$^* = ( ) - (\tilde{\ })$, A is the area enclosed, δl an increment of length along the boundary and C_n the velocity component normal to that boundary. The first term represents a heating effect which can occur when the mean inflowing air is at a different temperature from the interior, the second term is an "eddy" flux across the specified boundary, while the remaining terms retain their conventional meanings. Suppose for a moment that the instantaneous flow is always the same as the time-averaged flow (no transient motion). Then for this special coordinate system, $C_n = 0$ everywhere along this chosen boundary. Thus the

two boundary integral terms in Eq. (5.11) vanish for these circumstances. Note also from the divergence theorem that

$$\frac{\partial \bar{\omega}}{\partial p} = -\widetilde{\nabla_p \cdot \mathbf{V}_2} = A^{-1} \oint C_n \delta l = 0$$

because $C_n = 0$. However, the upper boundary condition for the model is $\omega = 0$ at $p = 0$. Therefore at the top level of the model, it follows that $\bar{\omega} = 0$ as well. This says that the only term remaining to balance the Q/c_p term (under these assumptions) is $[(R/c_p p) - \partial/\partial p]\widetilde{\omega^* T^*}$ (upon substitution of the equation of state to eliminate α). In the stratosphere, however, this term is very small, less than 0.05 K day^{-1}. On the other hand, Q/c_p in this calculation is about -0.3 K day^{-1}.

The above argument thus leads to a contradiction. The temperature is remaining essentially constant in the face of a substantial mean cooling, with no viable mechanism remaining to balance the loss. This dilemma leads to the conclusion that the assumption of complete stationarity is incorrect. In actual fact, when the model circulation relative to this coordinate is viewed on a daily basis, it becomes very evident that the term $A^{-1} \oint C_n'' T'' \delta l$ in Eq. (5.11) effects a substantial flux of heat across this coordinate axis into the polar vortex. Thus, the mean, Lagrangian-type circulation shown in Fig. 5.7 is not capable of an existence independent of transient disturbances.

This effect is also quite evident in the daily tracer behavior, particularly in the experiment described in MM78. When viewed instantaneously, the polar night jet of the model is continually reforming and dissipating. Associated with this transient behavior, "bursts" of air from lower latitudes penetrate irreversibly into the polar vortex region carrying relatively warmer temperatures and higher tracer amounts. Thus, even though the mid-stratospheric flow is relatively steady, nonsteady contributions are essential to account for the model time-mean structure of the thermal and tracer fields.

An additional consideration is that Andrews and McIntyre (1976, 1978b) showed that adiabatic, inviscid wave transience cannot by itself give rise to permanent alteration of mean flows. However, the results of Matsuno (1971) and Holton and Dunkerton (1978) demonstrate that wave transience in the presence of dissipation can substantially alter mean flows. Presumably, the ultimate role of wave transience in this GCM is to excite the dissipative and radiative processes which lead to irreversible tracer transport as well as permanent basic-state alteration. Earlier, this model showed that transient effects associated with seasonal flow transitions in the stratosphere can lead to very large decouplings of the usual large mean cell-eddy cancellations typical of midwinter flow regimes (MM78).

6. Summary

This work represents an attempt to provide a framework for a self-consistent 3-D model of ozone. The Stratified Tracer experiment incorporates no chemistry at all, but sets the 10 mb mixing ratio to a constant value. This provides an implicit ozone source for downward transport. The Simple Ozone experiment incorporates a simple, but physically plausible ozone chemistry at the 10 mb level only. Chemistry is not included at lower levels because of the substantial uncertainty in calculating the non-Chapman loss processes in a self-consistent manner. This calculation incorporates a single adjustable parameter, the 10 mb mixing ratio of total odd nitrogen.

In spite of the radical differences between the two experiments in the ozone source region, the lower stratosphere horizontal ozone structures in the two cases are remarkably similar to each other. This suggests strongly that the details of ozone chemistry in the middle stratosphere exert very little influence on the distribution of ozone in the lower stratosphere. An interesting difference, however, is that the global average ozone transport out of the middle stratosphere is less in the Simple Ozone experiment for the same global average vertical gradient. Thus, its effective 1-D "eddy diffusivity" is somewhat smaller. This behavior is consistent with the results of Mahlman (1976) which showed that the global-average vertical transport rate of a tracer is dependent on the local chemistry and the horizontal tracer structure, in addition to the global-average vertical gradient.

Although the Simple Ozone experiment shows qualitative agreement with observation in most respects, significant discrepancies remain. In the model Southern Hemisphere and tropics, the total ozone amounts are generally too small, while in Northern Hemisphere high latitudes they are somewhat too large. It is not yet clear whether these discrepancies are due mainly to the model's lack of chemistry in the lower stratosphere or to the model's overprediction of the interhemispheric differences in wintertime dynamical activity. As improvement of both of these effects would act to reduce the discrepancies, future experiments with improved model chemistry and dynamics are required to resolve this question.

Although the model cannot yet be used to calculate tropospheric ozone properly, evaluation of the ozone flux from stratosphere to troposphere is more reliable and is of considerable interest. The Simple Ozone experiment yielded a global annual average

flux across the tropopause of 5.1×10^{14} molecules $m^{-2} s^{-1}$, but with considerably larger fluxes in the Northern Hemisphere. The magnitude of the flux by eddies is calculated to be much larger than the flux by the meridional circulation.

In the same experiment, special attention is given to the processes leading to changes in the zonal-mean O_3 amounts at 10 mb. The results show a strong interaction between stratospheric transport and net chemical production or destruction in a particular region. In addition, the effect of a constantly changing sun angle combines with local temperature and transport effects to produce surprisingly complex behavior and interhemispheric asymmetries in the net chemical source and sink terms. These asymmetries act to produce large seasonal variations in the global-average mid-stratospheric O_3 production. Pronounced maxima appear during the winter months in each hemisphere, while net stratospheric O_3 destruction appears during the autumn months in each hemisphere.

In the Stratified Tracer experiment, the initial field was set to be horizontally uniform with a uniform vertical gradient. The early behavior of this experiment is used to evaluate the transport processes leading to the poleward-downward slopes of tracer isopleths in the lower stratosphere. The results showed the zonal-mean diabatic circulation to be a systematic contributor to the model's rapid evolution to poleward-downward slopes. Larger contributions are due to eddy processes, mainly vertical removal in low latitudes and horizontal buildup in higher latitudes. An additional calculation demonstrated that eddy diabatic processes are quite important for allowing systematic poleward-downward and equatorward-upward flux of air parcels across zonal-mean isentropic surfaces.

In an effort to simplify some of the interpretations of tracer transport phenomena, some aspects of Lagrangian perspectives are explored. A simple, but rather general, non-transport theorem is derived using a perspective which differs from that of Andrews and McIntyre (1976, 1978b) for their non-acceleration theorems. A calculation is performed of the isobaric drift of particles in a time-mean flow. The results show a systematic convergence of particles just to the cyclonic shear side of the time-mean non-zonal jet stream. Additionally, it is shown indirectly that the effect of transient disturbances in the lower stratosphere is of great importance for the irreversible transport of heat and tracers into the polar vortex region.

REFERENCES

Ackerman, M., 1971: Ultraviolet solar radiation related to mesospheric processes. *Mesospheric Models and Related Experiments*, D. Reidel, 149–159.

Aldaz, L., 1969: Flux measurements of atmospheric ozone over land and water. *J. Geophys. Res.*, **74**, 6943–6946.

Anderson, J. G., J. J. Margitan and F. Kaufman, 1974: Gas phase recombination of OH with NO and NO_2. *J. Chem. Phys.*, **60**, 3310–3317.

——, H. J. Grassl, R. E. Shetter and J. J. Margitan, 1980: Stratospheric free chlorine measured by balloonborne *in situ* resonance fluorescence. *J. Geophys. Res.* (in press).

Andrews, D. G., and M. E. McIntyre, 1976: Planetary waves in horizontal and vertical shear: The generalized Eliassen-Palm relation and the mean zonal acceleration. *J. Atmos. Sci.*, **33**, 2031–2048.

——, and ——, 1978a: Generalized Eliassen-Palm and Charney-Drazin theorems for waves in axisymmetric mean flows in compressible atmospheres. *J. Atmos. Sci.*, **35**, 175–185.

——, and ——, 1978b: An exact theory of nonlinear waves on a Lagrangian mean flow. *J. Fluid Mech.*, **89**, 609–646.

Boyd, J. P., 1976: The noninteraction of waves with the zonally averaged flow on a spherical earth and the interrelationships of eddy fluxes of energy, heat and momentum. *J. Atmos. Sci.*, **33**, 2285–2291.

Chameides, W. L., and J. C. G. Walker, 1973: A photochemical theory of tropospheric ozone. *J. Geophys. Res.*, **78**, 8751–8760.

Charney, J. G., and P. G. Drazin, 1961: Propagation of planetary-scale disturbances from the lower into the upper atmosphere. *J. Geophys. Res.*, **66**, 83–109.

Clark, J. H. E., 1970: A quasi-geostrophic model of the winter stratospheric circulation. *Mon. Wea. Rev.*, **98**, 443–461.

Crutzen, P. J., 1973: Gas-phase nitrogen and methane chemistry in the atmosphere. *Physics and Chemistry of the Upper Atmosphere*, B. McCormac, Ed., D. Reidel, 110–124.

Cunnold, D., F. Alyea, N. Phillips and R. Prinn, 1975: A three-dimensional dynamical-chemical model of atmospheric ozone. *J. Atmos. Sci.*, **32**, 170–194.

Danielsen, E. F., 1961: Trajectories: Isobaric, isentropic and actual. *J. Meteor.*, **18**, 479–486.

——, 1968: Stratospheric-tropospheric exchange based on radioactivity, ozone and potential vorticity. *J. Atmos. Sci.*, **25**, 502–518.

——, and V. Mohnen, 1977: Project duststorm report: Ozone transport, *in situ* measurements and meteorological analyses of tropopause folding. *J. Geophys. Res.*, **82**, 5867–5877.

Dickinson, R. E., 1969: Theory of planetary wave-zonal flow interaction. *J. Atmos. Sci.*, **26**, 73–81.

Dunkerton, T., 1978: On the mean meridional mass motions of the stratosphere and mesosphere. *J. Atmos. Sci.*, **35**, 2325–2333.

Dütsch, H. U., 1969: Atmospheric ozone and ultraviolet radiation. *World Survey of Climatology*, Vol. 4, *Climate of the Free Atmosphere*, D. F. Rex, Ed., Elsevier, 383–432.

——, 1974: Regular ozone soundings at the aerological station

of the Swiss Meteorological Office at Payerne, Switzerland, 1968–1972. Lapeth-10, Laboratorium für Atmosphärenphysik ETH, Zürich, 337 pp. [NTIS N75-2185415GA].

Eliassen, A., and E. Palm, 1960: On the transfer of energy in stationary mountain waves. *Geophys. Publ.*, **22**, 1–23.

Fabian, P., and C. Junge, 1970: Global rate of ozone destruction at the earth's surface. *Arch. Meteor. Geophys. Bioklim.*, **19**, 161–172.

Fishman, J., and P. J. Crutzen, 1978: The origin of ozone in the troposphere. *Nature*, **274**, 855–858.

Hampson, R. R., and D. Garvin, Eds., 1975: Chemical kinetic and photochemical data for modelling atmospheric chemistry. NBS Tech. Note 866, Washington, DC, 113 pp. [NTIS COM-75-10958/7GI].

Hayashi, Y., and D. G. Golder, 1977: Space-time spectral analysis of midlatitude disturbances appearing in a GFDL general circulation model. *J. Atmos. Sci.*, **34**, 237–262.

Heath, D. F., 1974: Recent advances in satellite observations of solar variability and global atmospheric ozone. NASA, Goddard Space Flight Center, X-912-74-190, 39 pp. [NTIS N74-30286/0GI].

Hering, W. S., 1965: Ozone and atmospheric transport processes. *Tellus*, **18**, 329–336.

—, and T. R. Borden, 1964: *Ozonesonde Observations over North America*, Vol. 2. AFCRL Environ. Res. Pap. No. 38, 280 pp. [NTIS AD 604 880].

—, and —, 1967: *Ozonesonde Observations over North America*, Vol. 4. AFCRL Environ. Res. Pap. No. 279, 365 pp. [NTIS AD-66 436].

Hochanadel, C. J., J. A. Ghormley and P. J. Ogren, 1972: Absorption spectrum and reaction kinetics of the HO_2 radical in the gas phase. *J. Chem. Phys.*, **56**, 4426–4432.

Holton, J. R., 1974: Forcing of mean flows by stationary waves. *J. Atmos. Sci.*, **31**, 942–945.

—, and T. Dunkerton, 1978: On the role of wave transience and dissipation in stratospheric mean flow oscillations. *J. Atmos. Sci.*, **35**, 740–744.

Howard, C. J., and K. M. Evenson, 1977: Kinetics of the reaction of HO_2 with NO. *Geophys. Res. Lett.*, **4**, 437–440.

Hudson, R. D., 1977: Chlorofluoromethanes and the stratosphere. NASA Ref. Publ. 1010, Washington, DC, 266 pp. [NTIS N77-31694/1GI].

Hunt, B. G., 1969: Experiments with a stratospheric general circulation model. III. Large-scale diffusion of ozone including photochemistry. *Mon. Wea. Rev.*, **97**, 287–306.

—, and S. Manabe, 1968: Experiments with a stratospheric general circulation model. II. Large-scale diffusion of tracers in the stratosphere. *Mon. Wea. Rev.*, **96**, 503–539.

Johnston, H., and R. Graham, 1973: Gas-phase ultraviolet absorption spectrum of nitric acid vapor. *J. Phys. Chem.*, **77**, 62–63.

Kao, S. K., C. N. Chi and W. M. Washington, 1976: Statistical characteristics of three-dimensional particle movement in the NCAR general circulation model. *J. Atmos. Sci.*, **33**, 1042–1049.

Kaufman, F., 1969: Neutral reactions involving hydrogen and other minor constituents. *Can. J. Chem.*, **47**, 1917–1924.

Kida, H., 1977a: A numerical investigation of the atmospheric general circulation and stratospheric-tropospheric mass exchange: I. Long-term integration of a simplified general circulation model. *J. Meteor. Soc. Japan*, **55**, 52–70.

—, 1977b: A numerical investigation of the atmospheric general circulation and stratospheric-tropospheric mass exchange: II. Lagrangian motion of the atmosphere. *J. Meteor. Soc. Japan*, **55**, 71–88.

Krishnamurti, T. N., 1961: The subtropical jet stream of winter. *J. Meteor.*, **18**, 172–191.

Kurzeja, R. J., 1975: The diurnal variations of minor constituents in the stratosphere and its effect on the ozone concentrations. *J. Atmos. Sci.*, **32**, 899–909.

Levy II, H., 1974: Photochemistry of the troposphere. *Advances in Photochemistry*, J. N. Pitts, Jr., G. S. Hammond and K. Gollnick, Eds., Wiley, 369–524.

—, J. D. Mahlman and W. J. Moxim, 1979: A preliminary report on the numerical simulation of the three-dimensional structure and variability of atmospheric N_2O. *Geophys. Res. Lett.*, **6**, 155–158.

London, J., 1963: The distribution of total ozone in the Northern Hemisphere. *Beitr. Phys. Atmos.*, **36**, 254–263.

—, and J. Park, 1973: Application of general circulation models to the study of stratospheric ozone. *Pure Appl. Geophys.*, **106–108**, 1611–1617.

—, and —, 1974: The interaction of ozone photochemistry and dynamics in the stratosphere: A three-dimensional atmospheric model. *Can. J. Chem.*, **52**, 1599–1609.

Lovill, J. E., 1974: A comparison of the Southern and Northern Hemisphere general circulation statistics as determined by satellite data. *Proc. Int. Conf. Structure, Composition and General Circulation of the Upper and Lower Atmospheres and Possible Anthropogenic Perturbations*, Vol. I., University of Melbourne, IAMAP, 340–359 [NTIS UCRL-75556].

Mahlman, J. D., 1969: Heat balance and mean meridional circulations in the polar stratosphere during the sudden warming of January 1958. *Mon. Wea. Rev.*, **97**, 534–540.

—, 1973a: Preliminary results from a three-dimensional general circulation/tracer model. *Proc. Second Conf. Climatic Impact Assessment Program*, A. J. Broderick, Ed., DOT-TSC-OST-73-4, 321–337 [NTIS PB-221 16612].

—, 1973b: On the maintenance of the polar front jet stream. *J. Atmos. Sci.*, **30**, 544–557.

—, 1976: Some fundamental limitations of simplified transport models as implied by results from a three-dimensional general-circulation/transport model. *Proc. Fourth Conf. Climatic Impact Assessment Program*, T. M. Hard and A. J. Broderick, Eds., DOT-TSC-OST-75-38, 132–146 [NTIS AD-A068982].

—, and W. J. Moxim, 1976: A method for calculating more accurate budget analyses of "sigma" coordinate model results. *Mon. Wea. Rev.*, **104**, 1102–1106.

—, and —, 1978: Tracer simulation using a global general circulation model: Results from a midlatitude instantaneous source experiment. *J. Atmos. Sci.*, **35**, 1340–1374.

Manabe, S., and J. L. Holloway, Jr., 1975: The seasonal variation of the hydrologic cycle as simulated by a global model of the atmosphere. *J. Geophys. Res.*, **80**, 1617–1649.

—, and J. D. Mahlman, 1976: Simulation of seasonal and interhemispheric variations in the stratospheric circulation. *J. Atmos. Sci.*, **33**, 2185–2217.

Matsuno, T., 1971: A dynamical model of the stratospheric sudden warming. *J. Atmos. Sci.*, **28**, 1479–1494.

—, and K. Nakumura, 1979: The Eulerian and Lagrangian mean meridional circulations in the stratosphere at the time of a sudden warming. *J. Atmos. Sci.*, **36**, 640–654.

Mintz, Y., and M. Schlesinger, 1976: Ozone production and transport with the UCLA general-circulation model. *Proc. Fourth Conf. Climatic Impact Assessment Program*, T. M. Hard and A. J. Broderick, Eds., DOT-TSC-OST-75-38, 201–222 [NTIS AD-A068982].

Murgatroyd, R. J., and F. Singleton, 1961: Possible meridional circulations in the stratosphere and mesosphere. *Quart. J. Roy. Meteor. Soc.*, **87**, 125–135.

Prabhakara, C., E. B. Rodgers, B. J. Conrath, R. A. Hanel and V. G. Kunde, 1976: The Nimbus 4 infrared spectroscopy experiment: 3. Observations of the lower stratospheric thermal structure and total ozone. *J. Geophys. Res.*, **81**, 6391–6399.

Reiter, E. R., 1971: *Atmospheric Transport Processes*. Part 2: *Chemical Tracers*. AEC Critical Review Series, 382 pp. [NTIS TID-25314].

Riehl, H., and D. Fultz, 1957: Jet stream and long waves in a steady rotating-dishpan experiment: Structure of the circulation. *Quart. J. Roy. Meteor. Soc.*, **83**, 215–231.

Schlesinger, M. E., and Y. Mintz, 1979: Numerical simulation of ozone production, transport and distribution with a global atmospheric general circulation model. *J. Atmos. Sci.*, **36**, 1325–1361.

Simon, P., 1974: Balloon measurements of solar fluxes between 1960Å and 2300Å. *Proc. Third Conf. Climatic Impact Assessment Program*, A. J. Broderick and T. Hard, Eds., DOT-TSC-OST-74-15, 137–142 [NTIS AD-A003 846/3GI].

Turco, R. P., R. C. Whitten, I. G. Poppoff and L. A. Capone, 1978: SST's, nitrogen fertilizer and stratospheric ozone. *Nature*, **276**, 805–807.

Wallace, J. M., 1978: Trajectory slopes, countergradient heat fluxes and mixing by lower stratospheric waves. *J. Atmos. Sci.*, **35**, 554–558.

Wofsy, S. C., 1974: Atmospheric photochemistry of N-, H-, and C-containing radicals. *Proc. Third Conf. Climatic Impact Assessment Program*, T. M. Hard and A. J. Broderick, Eds., DOT-TSC-OST-74-15, 359–375 [NTIS AD-A003 846/3GI].

——, 1978: Temporal and latitudinal variations of stratospheric trace gases: A critical comparison between theory and experiment. *J. Geophys. Res.*, **83**, 364–378.